Design of a Robust Adaptive Controller for a Hydraulic Press and Experimental Validation

Design of a Robust Adaptive Controller for a Hydraulic Press and Experimental Validation

Davide Barchi, Alessandro Macchelli, *Senior Member, IEEE*, Gildo Bosi, Lorenzo Marconi, *Fellow, IEEE*, Davide Foschi, and Mirco Mezzetti

***Abstract*— This paper aims to illustrate the design and validation of an adaptive controller developed for a hydraulic press. The controller architecture relies on an inner / outer loop structure, with an outer loop devoted to the control of the mechanical part, and the inner one of the hydraulic subsystem. Moreover, adaptive laws aiming to estimate / compensate for external forces and disturbances that occur during the pressing phase, and for leakage flow in the piston are present. This second estimate is used to maintain the performances acceptable in a wide set of operative conditions and for predictive maintenance. By using singular perturbation arguments, we show robustness to slowly increasing leakage gains, a typical situation in a real-world application. The control scheme is validated both on a simulative Simscape model and on the real hydraulic axis.**

***Index Terms*— hydraulic systems, adaptive control, backstepping control, nonlinear control, exponential stability, singular perturbations**

I. Introduction

THIS paper deals with the robust control of a hydraulic press that can be potentially used in many different industrial sectors. Such a system is characterised by nonlinear behaviour and by the presence of undesired elastic modes and delays that together with challenging tracking requirements, make the control quite complicated. Nonlinearity is mainly due to the fluid compressibility, to the servo-valve characteristic, and the elastic effects associated with the pipes. Also, the system is highly time-varying because of the wear-out of the hydraulic components, and it is typically subject to relevant external forces that can be treated as disturbances. Such forces have an order of magnitude of dozens of kilo-Newtons (kN), and are responsible for tracking and steady-state errors if not properly compensated. Similarly, the wear-out of the components causes an increase in time of the position error. This phenomenon is responsible for degraded performances in the production cycle causing very often the interruption of the machine to re-calibrate the controller. Besides, no information about the health of the hydraulic components is typically available, and so predictive maintenance is not usually applied.

D. Barchi, G. Bosi, D. Foschi and M. Mezzetti are with SACMI Imola S.C., via Selice Provinciale 17/a, 40026 Imola, Bologna, Italy. (e-mail: davide.barchi@sacmi.it, gildo.bosi@sacmi.it, davide.foschi@sacmi.it, mirco.mezzetti@sacmi.it)

A. Macchelli and L. Marconi are with the Department of Electrical, Electronic and Information Engineering (DEI), University of Bologna, viale del Risorgimento 2, 40136 Bologna, Italy. (e-mail: alessandro.macchelli@unibo.it, lorenzo.marconi@unibo.it)

The requirements that the controlled system has to meet are a maximum tracking error of $0.1 \div 0.5$ mm during the transient phase and a maximum steady-state error of one order of magnitude lower. Moreover, the maximum overshoot has to be lower than 1%. Now, such performances are typically obtained using a PID complemented with a feedforward action. The main issue, however, is that such severe requirements, in conjunction with the system non-idealities mentioned before, make the tuning of the controller quite difficult. In particular, most of the design of the feedforward action is carried out through experiments, and each hydraulic axis requires its tuning procedure. As a result, the controller is not robust against parameter variations, and the working cycle has to be interrupted once in a while to perform a re-calibration procedure. Because the press, for a given type of product, has to perform a large number of iterations of the same cycle, a possible solution could be to keep the actual PID controller and replace the feedforward action with a novel one obtained via iterative learning control (ILC), [1], [2], a design methodology that, in principle, is also capable to deal with several non-idealities in the plant such as unmodelled external forces, friction forces, fluid compressibility and leakage.

The idea of the paper, instead, is to move to a nonlinear adaptive control system that assures good performances in nominal working conditions, as well as in uncertain conditions when external forces and wear-out of the components are present. Moreover, if properly designed, the adaptive loop is capable to provide information about such non-ideal conditions that can be used for other scopes rather than stabilisation, e.g. for predictive maintenance. In this work, we are mainly driven by the adaptive robust control framework, [3], [4], and by the use of classical backstepping techniques, [5], [6]. Such techniques have been already successfully employed to control hydraulic systems, see e.g. [7]–[10], machine tools [11], robot manipulators [12], [13], and other engineering systems.

In particular, an inner / outer loop control strategy is adopted. The outer loop is responsible for controlling the motion of the press having the force applied to the piston as input, while the inner one for generating such pressure by acting on a servo-valve. On top of this scheme, two adaptive laws have been designed. The first one is associated with the outer loop and responsible for compensating not only the external forces that are generated during the pressing phase, but also all the unmodelled effects that act on the mechanical subsystem, such as friction, non-idealities in the pressure supply system, and fluid compressibility. On the other hand, the second adaptive

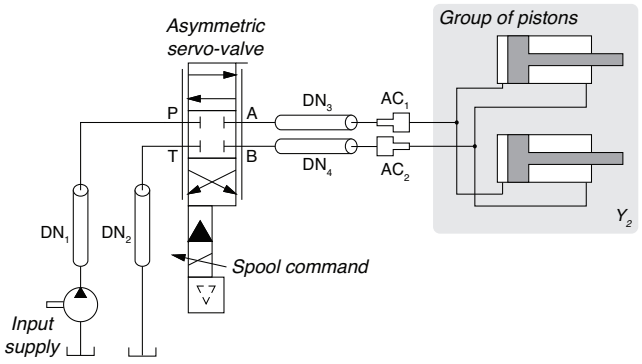

Fig. 1: Diagram of the Y_2-axis of the hydraulic press.

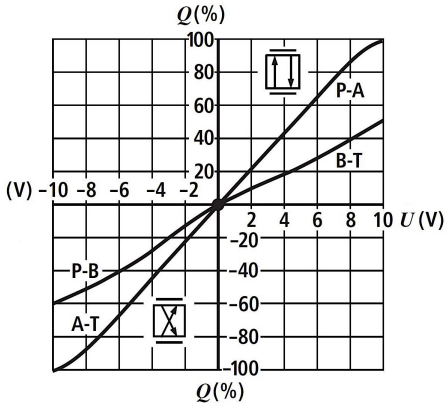

Fig. 2: Flow vs. command valve characteristic for the Y_2 axis. The command U is such that 10 V corresponds to the maximum displacement u for the spool that is equal to $u_{max} = 3$ mm. The maximum value for the flow, which corresponds to $Q = 100\%$, is 100 l/min.

law is devoted to reducing the performance degradation due to the wear-out of the components. Here, the focus is on the leakage flux in the piston. Such a phenomenon is time-varying but also characterised by dynamics that are largely slower than the ones associated with the working cycle of the press. By using the fact that the closed-loop system with the two adaptive laws is exponentially stable when the unknown parameters are constant, the control solution guarantees limited performance degradation when the leakage slowly increases. The result is proved via singular perturbations, see e.g. [14]. Note that the goal of the leakage estimator is twofold. It is employed not only to make the system robust against this effect but also to gather information for predictive maintenance about the internal state of the plant.

The paper is organised as follows. In Section II, the main characteristics and the mathematical model of the system are presented. A simulative model is developed within the MATLAB / Simscape environment to have a virtual benchmark at disposal to test the to-be-designed control law. Section III presents the control design, which relies on a simplified version of the model developed in the previous section. The performances of the obtained control law are then evaluated on the Simscape simulative model, in Section IV, where the validation of the model presented in Section II is also presented. Experimental results are then showed in Section V. Finally, conclusions and a brief overview of the future developments are discussed in Section VI.

II. System description & Modelling

The aim of this section is to illustrate the characteristics of the hydraulic axis, and to present two distinct models, one for control design and the other for verification purposes. The latter one is implemented in Simscape and experimentally validated in Section IV-A. The first model, instead, is derived from the "full-order" one by neglecting some "second order effects" that are not essential for control design.

A. Hydraulic axis description & Simscape model

In the press, 8 hydraulic axes moving in a synchronised manner are present. Even if different in size, maximum velocity and generated pressure, all the axes share a similar structure, schematically reported in Fig. 1. In this work, the focus is on a specific axis, referred to as Y_2, whose main components are:

- the pressure supply, responsible for providing a nominal pressure of 280 bar. Even if in the real application the working pressure is generated by a hydraulic subsystem composed by a pump, and by a chain of chambers minimising the pressure oscillations caused by the load, an ideal source able to supply the nominal pressure is employed in the Simscape model;
- the flexible pipes with circular section, denoted by DN_i, $i = 1, \ldots, 4$;
- resistive elements, denoted by AC_j, $j = 1, 2$, taking into account the interconnection between the piston chambers and the pipes;
- a group of 2 pistons in which compressibility effect of the fluid are taken into account;
- an asymmetric 4-ways servo-valve, to move the piston back and forth.

The servo-valves are zero-overlapped and the characteristic curve of the 4-ways valve used in the Y_2 axis is reported in Fig. 2. Note that the curve presents an asymmetric behaviour in the flow-to-voltage characteristics. Similarly to [15], this device is modelled by means of a custom Simscape component using 4 different orifices whose opening is related to the spool command via an algebraic map. As discussed also in Section IV-A, the algebraic relation used in the Simscape model has been determined by an optimisation procedure to fit the behaviour of the simulative model with experimental data collected on the real device. The servo-valve dynamics have been neglected since it is considerably faster than the hydraulic system. Due to its intrinsic nonlinear behaviour, the response of its linear approximation depends on the reference set-point. In particular, if the servo-valve command is around 5% of its maximum value, the associated transfer function is characterised by a pair of complex conjugated poles with a cutting frequency of about 60 Hz. Differently, if the servo-valve command is around 90% of its maximum value, the

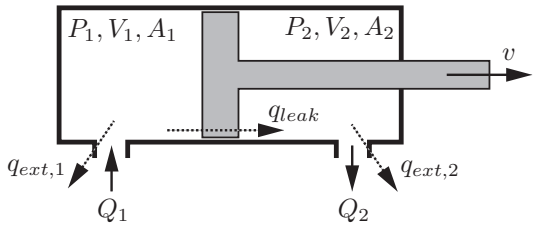

Fig. 3: Schematic representation of a 2-ways cylinder.

transfer function is characterised by a real pole, with cutting frequency around 20 Hz.

One of the main requirements for the control system is to identify and compensate for the leakage in the hydraulic circuit. Such a phenomenon is one of the most critical problems in hydraulic systems, and consists of an undesired fluid flow between two paths. It depends on several environmental conditions and on their time-evolution, and thus it is hard to be modelled. The focus here is on the leakage in the pistons that can be classified into two main types: the internal one, associated with a hydraulic flow between the two chambers, and the external one, associated with a fluid flow from one chamber to the environment. With reference to Fig. 3, in which a two-way piston is depicted, leakage is taken into account by adding in the ideal continuity equations the terms q_{leak} and $q_{ext,n}$, that model respectively internal and external leakages

$$\begin{cases} \dot{P}_1 = \dfrac{\beta_e}{V_1}(Q_1 - A_1 v - q_{leak} - q_{ext,1}) \\ \dot{P}_2 = \dfrac{\beta_e}{V_2}(-Q_2 + A_2 v + q_{leak} - q_{ext,2}) \end{cases} \tag{1}$$

In (1), V_1 and V_2 are the volumes of the two chambers, A_1 and A_2 the areas of the cylinder in each chamber, P_1 and P_2 the pressures, Q_1 and Q_2 the fluid flows, v the piston velocity, and β_e the bulk modulus of the fluid. For the sake of simplicity, only internal leakage has been taken into account, i.e. $q_{ext,1} = q_{ext,2} = 0$ in (1). It is also assumed that the internal leakage flow can be modelled as a time-varying orifice connecting the two chambers in the piston, namely

$$q_{leak} = C_{0l} x_l \sqrt{|P_1 - P_2|}\,\mathrm{sign}\,(P_1 - P_2). \tag{2}$$

Here, C_{0l} is the discharge gain of such orifice, and x_l is a "virtual displacement" that is proportional to the degree of severity of leakage.

Similar considerations can be drawn for the leakage flows in the valve. As discussed in [16], an expression along the same line of (2) to describe such flow in terms of the pressures in the system can be obtained. However, the final relation would be quite complex and so its use in an adaptive scheme would turn out to be not trivial at all.

B. Mathematical model for control design

Starting from the general description of Section II-A, a simplified mathematical representation of the Y_2 hydraulic axis is now obtained for control design. The plant consists of 2 cylinders operating in parallel, and a single valve. To simplify the model, only one piston is described, but with double areas, if compared to the ones used in the real device. This means that velocities, flow rates and pressures appearing in the model correspond to the "real" ones. From (1), we get

$$\begin{cases} \dot{x}_1(t) = x_2(t) \\ \dot{x}_2(t) = \dfrac{1}{m}\big[A_1 x_3(t) - A_2 x_4(t) - C_v x_2(t) - \\ \qquad\qquad - F_f(x_2(t))\big] + d(t) - g \\ \dot{x}_3(t) = \dfrac{\beta_e}{V_1(x_1(t))}\big[Q_1(x_3(t), u(t)) - \\ \qquad\qquad - A_1 x_2(t) - q_{leak}(t)\big] \\ \dot{x}_4(t) = \dfrac{\beta_e}{V_2(x_1(t))}\big[- Q_2(x_4(t), u(t)) + \\ \qquad\qquad + A_2 x_2(t) + q_{leak}(t)\big] \end{cases} \tag{3}$$

where:

- $x_1(t)$ and $x_2(t)$ are the cylinder position and velocity;
- m is the piston mass;
- C_v is the viscous friction coefficient;
- $F_f(x_2)$ takes into account unmodelled friction effects, with F_f unknown but Lipschitz-continuous;
- $d(t)$ are the unknown external disturbances / forces acting on the piston;
- g is the gravity acceleration;
- β_e is the bulk modulus of the fluid;
- A_1 and A_2 are the areas of the piston chambers;
- $x_3(t)$ and $x_4(t)$ are the pressures in the lower and upper chambers, i.e. P_1 and P_2 in (1), respectively;
- $V_1(x_1)$ and $V_2(x_1)$ are known functions that give the actual volumes of the lower and upper chambers, respectively;
- $u(t)$ is the spool displacement, i.e. the control input;
- $q_{leak}(t)$ is the unknown internal leakage flow;
- $Q_1(x_3, u)$ and $Q_2(x_4, u)$ are the input and output flow rates in the lower and upper chambers, respectively.

In (3), the control input is the spool displacement, which means that a static relation with the actual valve input command (a voltage) has been assumed. The spool displacement acts on the flows Q_1 and Q_2 of the lower and upper chambers. While in the reference Simscape model such relation has been realised by using 4 orifices and an algebraic map to match the valve characteristic, for control design, some simplifications are necessary. In particular, a linear relation for each line in the valve has been determined, and all the non-linear effects mentioned in Section II-A, as well as all the elastic phenomena, leakage flows, and the distinction between turbulent and laminar flow have been neglected.

Since the valve has an asymmetric behaviour, the flow rates Q_1 and Q_2 are asymmetric. It turns out that

$$\begin{aligned} Q_1(x_3, u) &= C_{01} u \sqrt{|\Delta P_1|}\,\mathrm{sign}(\Delta P_1) \\ Q_2(x_4, u) &= C_{02} u \sqrt{|\Delta P_2|}\,\mathrm{sign}(\Delta P_2) \end{aligned} \tag{4}$$

where

$$\begin{aligned} \Delta P_1 &= \begin{cases} P_s - x_3 & \text{if } u \geq 0 \\ x_3 - P_r & \text{if } u < 0 \end{cases} \\ \Delta P_2 &= \begin{cases} x_4 - P_r & \text{if } u \geq 0 \\ P_s - x_4 & \text{if } u < 0. \end{cases} \end{aligned} \tag{5}$$

Here, $P_s = 280\,\text{bar}$ is the supplied pressure, $P_r = 0\,\text{bar}$ is the reference (environment) pressure, and C_{01} and C_{02} are the flow rate gains of the valve. These constants are estimated at the nominal flow rates Q_{N1} and Q_{N2}, respectively, and at the nominal pressure drop $\Delta P_N = 10\,\text{bar}$, by thus obtaining

$$C_{01} = \frac{Q_{N1}}{u_{max}\sqrt{\Delta P_N}} \qquad C_{02} = \frac{Q_{N2}}{u_{max}\sqrt{\Delta P_N}} \tag{6}$$

where $u_{max} = 3\,\text{mm}$ is the maximum spool opening. The asymmetric behaviour of the valve is described by acting on the nominal flows Q_{N1} and Q_{N2}, i.e. by imposing that

$$Q_{N1} = \begin{cases} Q_N^{PA} & \text{if } u \geq 0 \\ Q_N^{PB} & \text{if } u < 0 \end{cases} \quad Q_{N2} = \begin{cases} Q_N^{BT} & \text{if } u \geq 0 \\ Q_N^{AT} & \text{if } u < 0 \end{cases}$$

where Q_N^{PA}, Q_N^{BT}, Q_N^{PB} and Q_N^{AT} are the nominal flow rates for each orifice, which depend on the spool position. Such values have been tuned via a quadratic optimisation problem to match the real characteristic of the valve. The idea is to use this information for control design, so this is a good compromise between accuracy and simplicity. With Fig. 2 in mind, at the nominal flow rate $Q_N = 100\,\text{l/min}$, we get that $Q_N^{PA} = Q_N^{AT} = 100\,\text{l/min}$, $Q_N^{BT} = 50\,\text{l/min}$, and $Q_N^{PB} = 60\,\text{l/min}$.

III. Control design

The aim of this section is to show how to design a robust and adaptive control system for (3) that is able to dynamically react against high magnitude external disturbances $d(t)$ generated during the pressing process, and also able to compensate the offset caused by the slowly varying internal leakage flow $q_{leak}(t)$. A reliable estimate of the latter quantity is also necessary for diagnostic and maintenance purposes. From (3) and (4), the plant is described by:

$$\begin{cases} \dot{x}_1 = x_2 \\ \dot{x}_2 = \dfrac{1}{m}\big[A_1 x_3 - A_2 x_4 - C_v x_2 - \\ \qquad\qquad - F_f(x_2)\big] + d - g \\ \dot{x}_3 = \dfrac{\beta_e}{V_1(x_1)}\big[C_{01} u \sqrt{|\Delta P_1|}\,\text{sign}\,\Delta P_1 - \\ \qquad\qquad - A_1 x_2 - q_{leak}\big] \\ \dot{x}_4 = \dfrac{\beta_e}{V_2(x_1)}\big[- C_{02} u \sqrt{|\Delta P_2|}\,\text{sign}\,\Delta P_2 + \\ \qquad\qquad + A_2 x_2 + q_{leak}\big] \end{cases} \tag{7}$$

where $V_1(x_1) = V_{01} + A_1 x_1$, $V_2(x_1) = V_{02} - A_2 x_1$, and ΔP_1 and ΔP_2 are defined in (5). Let $x_1^\star(t)$ be a desired reference trajectory for the piston defining the nominal working cycle, and let $x_2^\star(t) := \dot{x}_1^\star(t)$ be the associated velocity profile. The following assumptions are then made:

- the parameters C_v, C_{01}, C_{02}, m, β_e, A_1, A_2, V_{01} and V_{02} are known and constant. In this paper, only an experimentally determined estimate of the viscous friction coefficient C_v is employed in control design.
- The function F_f is increasing and globally Lipschitz, i.e. for all x_a and x_b there exists $\bar{F} > 0$ such that

$$\begin{aligned} (x_b - x_a)\big[F_f(x_b) - F_f(x_a)\big] &\geq 0 \\ |F_f(x_b) - F_f(x_a)| &\leq \bar{F}|x_b - x_a| \end{aligned} \tag{8}$$

  For any reference velocity profile $x_2^\star(t)$ we have that

$$F_f(x_2^\star(t)) = \sum_{i=1}^{N_f} \phi_i \Phi_i(x_2^\star(t)) \tag{9}$$

  where $\Phi_i(x_2^\star)$ is a known and bounded function, and ϕ_i is a real and unknown constant, with $i = 1, \ldots, N_f$. The functions Φ_i are bounded and of class C^1. They are selected so that (9) could describe e.g. dry and viscous friction forces. Note that stiction does not meet the first requirement in (8), so it cannot be included in the friction model. Its influence on the dynamics is taken into account in the term $d(t)$.
- For any reference trajectory $x_1^\star(t)$, there exist a set of known and bounded functions $\Gamma_i(t)$, a set of unknown parameters γ_i, $i = 1, \ldots, N_d$, and a know and bounded function $F_{ext}(x_1)$ such that

$$d(t) = F_{ext}(x_1(t)) + d_\gamma(t) \tag{10}$$

  being

$$d_\gamma(t) := \sum_{i=1}^{N_d} \gamma_i \Gamma_i(t). \tag{11}$$

  Since the working cycle is periodic, namely it is based on the periodic repetition of the reference trajectory $x_1^\star(t)$, the functions Γ_i and thus d_γ are assumed to be bounded, of class C^1 and periodic.
- As for the internal leakage, based on (2), we assume that

$$q_{leak}(t) = g_l(t) G_l(x_3(t), x_4(t)) \tag{12}$$

  in which $G_l(x_3, x_4) := \sqrt{|x_3 - x_4|}\,\text{sign}\,(x_3 - x_4)$ and $g_l(t) := C_{0l} x_l(t)$; $g_l(t)$ is a time-varying "leakage gain," which is bounded and unknown. Since the dynamics associated to the change in the leakage flow is much slower than the hydraulic system dynamics, we have that $0 < \dot{g}_l(t)$ and bounded, and such that $\dot{g}_l(t) \simeq 0$.
- The full state vector $x = (x_1, x_2, x_3, x_4)$ is measurable.

As discussed in [17], let $\bar{x}_3 := A_1 x_3 - A_2 x_4$ denote the total force acting on the piston. The design of the control system is based on a "reduced system" with state variables $(x_1, x_2, \bar{x}_3)$ that from (7) reads as

$$\begin{cases} \dot{x}_1 = x_2 \\ \dot{x}_2 = \dfrac{1}{m}\big[\bar{x}_3 - C_v x_2 - F_f(x_2)\big] + d - g \\ \dot{\bar{x}}_3 = f_1(x) u - f_2(x_1) x_2 - f_3(x_1) q_{leak} \end{cases} \tag{13}$$

where

$$\begin{aligned} f_1(x) &:= \frac{\beta_e A_1}{V_1(x_1)} C_{01} \sqrt{|\Delta P_1|}\,\text{sign}\,\Delta P_1 + \\ &\quad + \frac{\beta_e A_2}{V_2(x_1)} C_{02} \sqrt{|\Delta P_2|}\,\text{sign}\,\Delta P_2 \\ f_2(x_1) &:= \beta_e \left[\frac{A_1^2}{V_1(x_1)} + \frac{A_2^2}{V_2(x_1)}\right] \\ f_3(x_1) &:= \beta_e \left[\frac{A_1}{V_1(x_1)} + \frac{A_2}{V_2(x_1)}\right]. \end{aligned}$$

This system is in semi-strict-feedback form, [14], [18].

We face the problem of letting the state (x_1, x_2) of (13) to track the reference signal $(x_1^\star, x_2^\star)$. To achieve this, we start by considering the first two dynamics regarded as a second order system with state (x_1, x_2) and virtual control input $\bar{x}_3$. As a matter of fact, since the control design is based on (13), the pressures inside the piston, i.e. x_3 and x_4 (7), are not required to track some desired profile independently one from the other. Consequently, as in [17], [19], it is necessary to assume that such pressures evolve within the set $[P_r, P_s]$. Note that since $x_4(t)$ is measured, it can be regarded in (13) as a measurable input. The same property holds also for $x_3(t)$.

Assumption 3.1: Given the reference trajectory $x_1^\star(t)$, system (7) is such that $P_r \leq x_3(t) \leq P_s$ and $P_r \leq x_4(t) \leq P_s$.

By defining the error coordinates

$$z_1(t) := x_1(t) - x_1^\star(t) \qquad z_2(t) := x_2(t) - x_2^\star(t)$$

the system in question reads as

$$\begin{cases} \dot{z}_1 = z_2 \\ \dot{z}_2 = \dfrac{1}{m}\big[\bar{u} - C_v(z_2 + x_2^\star) - F_f(z_2 + x_2^\star)\big] + \\ \qquad\qquad + F_{ext}(z_1 + x_1^\star) + d_\gamma - g \end{cases} \tag{14}$$

in which we denoted by $\bar{u}$ the state variable $\bar{x}_3$ to emphasise the fact the latter is regarded as virtual input for (14). For this system, a feedback linearising control action $\bar{u}(t)$ that makes the origin of (14) globally exponentially stable when $F_f(x_2) = 0$ and $d_\gamma(t) = 0$ can be simply obtained. Such control action is given by

$$\bar{u} = -m\big[K_1 z_1 + K_2 z_2 + F_{ext}(z_1 + x_1^\star) - g\big] + \\ + C_v(z_2 + x_2^\star) \tag{15}$$

with K_1, $K_2 > 0$. The next proposition builds on (15) to present an adaptive control law that makes the origin of (14) globally exponentially stable when $F_f(x_2)$ and $d_\gamma(t)$ are present. Before presenting the result, we make the following assumption.

Assumption 3.2: Consider the functions $F_f(x_2^\star(t))$ and $d_\gamma(t)$ introduced in (9) and in (11), respectively, and let

$$\Theta(t) := \begin{pmatrix} \frac{1}{m}\Phi_1(x_2^\star(t)) \\ \vdots \\ \frac{1}{m}\Phi_{N_f}(x_2^\star(t)) \\ -\Gamma_1(t) \\ \vdots \\ -\Gamma_{N_d}(t) \end{pmatrix}. \tag{16}$$

The entries of $\Theta : \mathbb{R}_+ \to \mathbb{R}^{N_f+N_d}$ are C^1, and there exists positive constants D_0 and D_1 such that

$$\max_{t\in\mathbb{R}_+} \|\Theta(t)\| \leq D_0 \qquad \max_{t\in\mathbb{R}_+} \left\|\dot{\Theta}(t)\right\| \leq D_1 \tag{17}$$

where $\|\cdot\|$ denotes the Euclidean norm. Moreover, there exists positive constants μ and T such that

$$\int_{t-T}^{t} \Theta(\tau)\Theta^{\mathrm{T}}(\tau)\,\mathrm{d}\tau \geq \mu I \tag{18}$$

for all $t \geq T$. This last requirement is a classical persistency of excitation condition, [20].

With (16) in mind, let

$$\theta := \begin{pmatrix} \phi_1 & \dots & \phi_{N_f} & \gamma_1 & \dots & \gamma_{N_d} \end{pmatrix}^{\mathrm{T}} \tag{19}$$

and note that the second equation in (14) can be rewritten as

$$\dot{z}_2 = \frac{1}{m}\big[\bar{u} - C_v(z_2 + x_2^\star) - F_f(z_2 + x_2^\star) + F_f(x_2^\star)\big] + \\ + F_{ext}(z_1 + x_1^\star) - g - \frac{1}{m}F_f(x_2^\star) + d_\gamma.$$

System (14) thus becomes (see (9) and (11))

$$\begin{cases} \dot{z}_1 = z_2 \\ \dot{z}_2 = -\dfrac{1}{m}\big[C_v(z_2 + x_2^\star) + F_f(z_2 + x_2^\star) - F_f(x_2^\star)\big] + \\ \qquad\qquad + F_{ext}(z_1 + x_1^\star) - g - \theta^{\mathrm{T}}\Theta + \dfrac{1}{m}\bar{u} \end{cases} \tag{20}$$

in which we used the fact that $\frac{1}{m}F_f - \sum_{i=1}^{N_d}\gamma_i\Gamma_i = \theta^{\mathrm{T}}\Theta$ because of (16) and (19). Let $\hat{\theta} \in \mathbb{R}^{N_f+N_d}$ denote the estimate of θ defined in (19). In the next proposition, we show that the control action

$$\bar{u} = -m\big[K_1 z_1 + K_2 z_2 + F_{ext}(z_1 + x_1^\star) - g\big] + \\ + C_v(z_2 + x_2^\star) + m\hat{\theta}^{\mathrm{T}}\Theta \tag{21}$$

and the adaptive law

$$\dot{\hat{\theta}}(t) = -\big[\varepsilon_1 z_1(t) + z_2(t)\big]K_\theta\Theta(t) \tag{22}$$

make the trajectories of (20) to converge to $(0, 0, \theta)$ globally, uniformly and exponentially, [14, Definition 3.5]. In (22), K_θ is a $(N_f + N_d) \times (N_f + N_d)$ symmetric and positive definite real matrix.

Proposition 3.1: Consider the system (20) and suppose that Assumption 3.2 holds true. Let ε_1, δ_2, δ_3 and δ_4 denote positive constants selected so that $\frac{\mu}{T} > \bar{\Gamma}_\theta$, where

$$\bar{\Gamma}_\theta := \frac{1}{2}\left(\varepsilon_1\delta_2 D_1 + \delta_4\bar{\Gamma}_2'\right) + \frac{D_0^2}{\delta_3}, \tag{23}$$

being

$$\bar{\Gamma}_2' := T\,\|K_\theta\|\,D_0^3 + D_1 + \left(\varepsilon_1 + \frac{\bar{F}}{m}\right)D_0 \tag{24}$$

and $\bar{F} > 0$ a constant so that (8) holds. Besides, let K_1 and K_2 denote positive gains, K_θ a symmetric and positive definite real matrix, and ε_2 and δ_1 positive constants selected so that

$$K_1 > \bar{\Gamma}_1 + \frac{\varepsilon_2\delta_3 K_1^2}{2\varepsilon_1} \qquad K_2 > \bar{\Gamma}_2 + \frac{\varepsilon_2\delta_3 K_2^2}{2} \tag{25}$$

where

$$\bar{\Gamma}_1 := \frac{\delta_1\bar{F}}{2m} + 2\varepsilon_1\varepsilon_2\,\|K_\theta\|\,D_0^2 + \frac{\varepsilon_2 D_1}{2\delta_2} \\ \bar{\Gamma}_2 := \varepsilon_1\left(1 + \frac{\bar{F}}{2\delta_1 m}\right) + 2\varepsilon_2\,\|K_\theta\|\,D_0^2 + \frac{\varepsilon_2\bar{\Gamma}_2'}{2\delta_4}. \tag{26}$$

Then, the trajectories of the closed-loop system resulting from (20) with control action (21) and adaptive law (22) are bounded, and $(z_1(t), z_2(t), \hat{\theta}(t)))$ converges to $(0, 0, \theta)$ globally, uniformly and exponentially.

Proof: The closed-loop system obtained from (20), (21) and (22) reads as

$$\begin{cases} \dot{z}_1 = z_2 \\ \dot{z}_2 = -K_1 z_1 - K_2 z_2 + \tilde{\theta}^{\mathrm{T}}\Theta - \\ \qquad\qquad - \dfrac{1}{m}\left[F_f(z_2 + x_2^\star) - F_f(x_2^\star)\right] \\ \dot{\tilde{\theta}} = u_\theta \end{cases} \tag{27}$$

where $\tilde{\theta} := \hat{\theta} - \theta$. Given a sufficiently small $\varepsilon_1 > 0$, consider the Lyapunov function

$$V_1(z_1, z_2, \tilde{\theta}) := \frac{1}{2}(K_1 + \varepsilon_1 K_2) z_1^2 + \frac{1}{2} z_2^2 + \\ + \varepsilon_1 z_1 z_2 + \frac{1}{2}\tilde{\theta}^{\mathrm{T}} K_\theta^{-1} \tilde{\theta} \tag{28}$$

in which $K_\theta = K_\theta^{\mathrm{T}} > 0$. Along the trajectories of (27), we have that

$$\dot{V}_1(z_1, z_2, \tilde{\theta}) = -\varepsilon_1 K_1 z_1^2 - (K_2 - \varepsilon_1) z_2^2 + \\ + (\varepsilon_1 z_1 + z_2)\tilde{\theta}^{\mathrm{T}}\Theta + \tilde{\theta}^{\mathrm{T}} K_\theta^{-1} u_\theta - \\ - \frac{1}{m}(\varepsilon_1 z_1 + z_2)\left[F_f(z_2 + x_2^\star) - F_f(x_2^\star)\right]. \tag{29}$$

With the indicated choice of u_θ, (29) becomes

$$\dot{V}_1(z_1, z_2, \tilde{\theta}) = -\varepsilon_1 K_1 z_1^2 - (K_2 - \varepsilon_1) z_2^2 - \\ - \frac{1}{m}(\varepsilon_1 z_1 + z_2)\left[F_f(z_2 + x_2^\star) - F_f(x_2^\star)\right].$$

Since F_f is increasing and globally Lipschitz, and $x_2^\star(t)$ is bounded, from (8), we have that $z_2\left[F_f(z_2 + x_2^\star) - F_f(x_2^\star)\right] \geq 0$ and $|F_f(z_2 + x_2^\star) - F_f(x_2^\star)| \leq \bar{F}|z_2|$ for some $\bar{F} > 0$ and all z_2. This implies that

$$\dot{V}_1(z_1, z_2, \tilde{\theta}) \leq -\varepsilon_1 K_1 z_1^2 - (K_2 - \varepsilon_1) z_2^2 + \frac{\varepsilon_1 \bar{F}}{m}|z_1 z_2|$$

and, by using the Young's inequality, that

$$\dot{V}_1(z_1, z_2, \tilde{\theta}) \leq -\varepsilon_1 \left(K_1 - \frac{\delta_1 \bar{F}}{2m}\right) z_1^2 - \\ - \left[K_2 - \varepsilon_1\left(1 + \frac{\bar{F}}{2\delta_1 m}\right)\right] z_2^2 \tag{30}$$

where δ_1 is an arbitrary positive number. By the indicated choices of K_1 and K_2 with $\varepsilon_2 = 0$, then $\dot{V}_1(z_1, z_2, \tilde{\theta}) \leq 0$. This fact implies that the trajectories of (27) are bounded. To prove global exponential convergence towards the origin of (27), we follow [21]. Let us consider the functions

$$V_2(z_1, z_2, \tilde{\theta}) := \tilde{\theta}^{\mathrm{T}}\Theta(\varepsilon_1 z_1 + z_2), \tag{31}$$

$$V_3(\tilde{\theta}) := \frac{1}{T}\tilde{\theta}^{\mathrm{T}}\left[\int_{t-T}^{t}\int_{\bar{\tau}}^{t} \Theta(\tau)\Theta^{\mathrm{T}}(\tau)\,\mathrm{d}\tau\,\mathrm{d}\bar{\tau}\right]\tilde{\theta}. \tag{32}$$

Along the trajectories of (27), we have that

$$\dot{V}_2(z_1, z_2, \tilde{\theta}) = \\ = \tilde{\theta}^{\mathrm{T}}\dot{\Theta}(\varepsilon_1 z_1 + z_2) - (\varepsilon_1 z_1 + z_2)^2 \Theta^{\mathrm{T}} K_\theta \Theta + \\ + \tilde{\theta}^{\mathrm{T}}\Theta\left(\varepsilon_1 z_2 - K_1 z_1 - K_2 z_2\right) + \left(\tilde{\theta}^{\mathrm{T}}\Theta\right)^2 - \\ - \frac{1}{m}\tilde{\theta}^{\mathrm{T}}\Theta\left[F_f(z_2 + x_2^\star) - F_f(x_2^\star)\right] \tag{33}$$

while for (32) we have that

$$\dot{V}_3(\tilde{\theta}) = -\frac{2}{T}\tilde{\theta}^{\mathrm{T}}\left[\int_{t-T}^{t}\int_{\bar{\tau}}^{t} \Theta(\tau)\Theta^{\mathrm{T}}(\tau)\,\mathrm{d}\tau\,\mathrm{d}\bar{\tau}\right]\cdot \\ \cdot (\varepsilon_1 z_1 + z_2) K_\theta \Theta + \left(\tilde{\theta}^{\mathrm{T}}\Theta\right)^2 - \\ - \frac{1}{T}\tilde{\theta}^{\mathrm{T}}\left[\int_{t-T}^{t} \Theta(\tau)\Theta(\tau)^{\mathrm{T}}\,\mathrm{d}\tau\right]\tilde{\theta} \\ \leq T\left\|K_\theta\right\| D_0^3 \left\|\tilde{\theta}\right\| |z_2| + \left(\tilde{\theta}^{\mathrm{T}}\Theta\right)^2 - \frac{\mu}{T}\left\|\tilde{\theta}\right\|^2 \tag{34}$$

where the first condition in (17) and assumption (18) have been taken into account. Now, with (28), (31) and (32) in mind, let us introduce the function

$$W_1(z_1, z_2, \tilde{\theta}) := V_1(z_1, z_2, \tilde{\theta}) - \varepsilon_2 V_2(z_1, z_2, \tilde{\theta}) + \varepsilon_2 V_3(\tilde{\theta})$$

for which it is easy to check that, if $\varepsilon_1, \varepsilon_2 > 0$ are sufficiently small, there exist $\alpha_1, \alpha_2 > 0$ such that

$$\alpha_1 \left\|\begin{pmatrix} z_1 & z_2 & \tilde{\theta}\end{pmatrix}^{\mathrm{T}}\right\|^2 \leq W_1(z_1, z_2, \tilde{\theta}) \leq \\ \leq \alpha_2 \left\|\begin{pmatrix} z_1 & z_2 & \tilde{\theta}\end{pmatrix}^{\mathrm{T}}\right\|^2. \tag{35}$$

Along the trajectories of (27) and having in mind the bounds defined in (17), from (30), (33) and (34), we have that

$$\dot{W}_1(z_1, z_2, \tilde{\theta}) \leq -\varepsilon_1\left(K_1 - \frac{\delta_1 \bar{F}}{2m} - 2\varepsilon_1\varepsilon_2\left\|K_\theta\right\| D_0^2\right) z_1^2 - \\ - \left[K_2 - \varepsilon_1\left(1 + \frac{\bar{F}}{2\delta_1 m}\right) - 2\varepsilon_2\left\|K_\theta\right\| D_0^2\right] z_2^2 - \\ - \frac{\varepsilon_2\mu}{T}\left\|\tilde{\theta}\right\|^2 + \varepsilon_2\left(\varepsilon_1 D_1 + K_1 D_0\right)\left\|\tilde{\theta}\right\| |z_1| + \\ + \varepsilon_2\left(\bar{\Gamma}_2' + K_2 D_0\right)\left\|\tilde{\theta}\right\| |z_2|$$

since $(\varepsilon_1 z_1 + z_2)^2 \leq 2(\varepsilon_1^2 z_1^2 + z_2^2)$, and where $\bar{\Gamma}_2'$ is defined in (24). By using the Young's inequality, we finally obtain that

$$\dot{W}_1(z_1, z_2, \tilde{\xi}_\theta) \leq -\Gamma_1 z_1^2 - \Gamma_2 z_2^2 - \varepsilon_2\Gamma_\theta\left\|\tilde{\theta}\right\|^2 \tag{36}$$

where

$$\Gamma_1 := \varepsilon_1 K_1 - \varepsilon_1\bar{\Gamma}_1 - \frac{\varepsilon_2\delta_3 K_1^2}{2} \\ \Gamma_2 := K_2 - \bar{\Gamma}_2 - \frac{\varepsilon_2\delta_3 K_2^2}{2} \\ \Gamma_\theta := \frac{\mu}{T} - \bar{\Gamma}_\theta \tag{37}$$

with $\bar{\Gamma}_1$ and $\bar{\Gamma}_2$ defined in (26), and $\bar{\Gamma}_\theta$ in (23). If K_1 and K_2 are selected so that (25) holds, and if the constants ε_1, ε_2 and δ_i, $i = 1, \ldots, 4$, are chosen so that the hypotheses of the proposition are met, we have that the gains defined in (37) are positive. As a consequence, from (36), if $\Gamma := \min\{\Gamma_1, \Gamma_2, \varepsilon_2\Gamma_\theta\}$, we obtain that

$$\dot{W}_1(z_1, z_2, \tilde{\xi}_\theta) \leq -\Gamma\left\|\begin{pmatrix} z_1 & z_2 & \tilde{\theta}\end{pmatrix}^{\mathrm{T}}\right\|^2, \qquad \Gamma > 0. \tag{38}$$

To prove that $(z_1(t), z_2(t), \tilde{\theta}(t))$ globally converges to zero exponentially and uniformly in the initial conditions we rely on [14, Corollary 3.4], from which the result follows since (35) and (38) hold for some $\alpha_1, \alpha_2, \Gamma > 0$. ■

The previous result provides the expression (21) for the "virtual" control input $\bar{x}_3(t)$ that assures that the mechanical subsystem in (13) exponentially tracks a desired reference trajectory $x_1^\star(t)$. By following the standard backstepping procedure, we compute now the true input $u(t)$. The goal is to back-step by preserving robustness to the disturbances affecting the mechanical dynamics and to $q_{leak}(t)$. By letting

$$z_3(t) := \bar{x}_3(t) - \bar{u}(t)$$

we obtain

$$\begin{cases} \dot{z}_1 = z_2 \\ \dot{z}_2 = \dfrac{1}{m}\big[z_3 + \bar{u} - C_v(z_2 + x_2^\star) - F_f(z_2 + x_2^\star)\big] + \\ \qquad\qquad + F_{ext}(z_1 + x_1^\star) + d_\gamma - g \\ \dot{z}_3 = f_1'(z_e,t)u - f_2'(z_1,t)z_2 - f_3'(z_1,t)q_{leak} - \\ \qquad\qquad - f_2'(z_1,t)x_2^\star - \dot{\bar{u}} \end{cases} \tag{39}$$

where (14) has been taken into account, and $f_1'(z_e,t)$, $f_2'(z_1,t)$ and $f_3'(z_1,t)$ are the functions $f_1(x)$, $f_2(x_1)$ and $f_3(x_1)$ in (13) in the new error coordinates, with $z_e := (z_1, z_2, z_3, x_4)$.

The next proposition presents an adaptive control law by assuming that the internal leakage takes the form (12), and that the "leakage gain" $g_l(t)$ is constant. In this case, global exponential stability is proved. The case in which $g_l(t)$ varies very slowly if compared to the dynamics of the system and the reference trajectory is treated later. Similarly to Proposition 3.1, we make the following assumption.

Assumption 3.3: Consider $q_{leak}(t)$ given by (12), in which $G_l(x_3, x_4)$ is a known function and $g_l(t) \equiv \bar{g}_l \geq 0$, but unknown, and the function $f_3'(z_1,t)$ is introduced in (39). Define

$$\Theta_l(t) := G_l'(z_e(t),t) f_3'(z_1(t),t) \tag{40}$$

where $G_l'(z_e,t)$ is the function $G_l(x_3,x_4)$ in the new error coordinates, with $z_e = (z_1, z_2, z_3, x_4)$. Similarly to Assumption 3.2, suppose that Θ_l is of class C^1 and that there exists positive constants L_0 and L_1 such that

$$\max_{t\in\mathbb{R}_+} |\Theta_l(t)| \leq L_0 \qquad \max_{t\in\mathbb{R}_+} \left|\dot{\Theta}_l(t)\right| \leq L_1. \tag{41}$$

Moreover, suppose that there exists positive constants μ_l and T_l such that

$$\int_{t-T_l}^{t} \Theta_l^2(\tau)\,\mathrm{d}\tau \geq \mu_l \tag{42}$$

for all $t \geq T_l$.

Let $\hat{g}_l \in \mathbb{R}$ denote the estimate of g_l introduced in (12). With an eye on Proposition 3.1, we show that the control action

$$u = \frac{1}{f_1'(z_e,t)}\Big[-\frac{z_2}{m} - K_3 z_3 + \dot{\bar{u}} + \\ + f_2'(z_1,t)(z_2 + x_2^\star) + \hat{g}_l G_l'(z_e,t) f_3'(z_1,t)\Big] \tag{43}$$

where $\bar{u}$ is given by (21), and the adaptive laws (22) and

$$\dot{\hat{g}}_l = -K_l G_l'(z_e,t) f_3'(z_1,t) z_3 \tag{44}$$

make the trajectories of (39) to converge to $(0,0,0,\theta,\bar{g}_l)$ globally, uniformly and exponentially.

Proposition 3.2: Consider the system (39) and suppose that Assumptions 3.2 and 3.3 hold true. Let K_l denote a positive gain, and ε_1, δ_2, δ_3, δ_4, δ_6, δ_7, δ_8 and δ_9 positive constants selected so that

$$\frac{\mu}{T} > \bar{\Gamma}_\theta + \frac{\delta_6 D_0}{2m} \qquad \frac{\mu_l}{T_l} > \frac{1}{2}\left(\frac{L_0\delta_7}{m} + \bar{\Gamma}_3\delta_8 + \frac{1}{\delta_9}\right) \tag{45}$$

with $\bar{\Gamma}_\theta$ defined in (23),

$$\bar{\Gamma}_3 := T_l K_l L_0^3 + L_1 \tag{46}$$

and $\bar{F} > 0$ a sufficiently large constant so that (8) holds. Besides, let K_1, K_2 and K_3 denote positive gains, K_θ a symmetric and positive definite real matrix, and ε_2, ε_3, δ_1 and δ_5 positive constants selected so that

$$\begin{aligned} K_1 &> \bar{\Gamma}_1 + \frac{\delta_5}{2m} + \frac{\varepsilon_2\delta_3 K_1^2}{2\varepsilon_1} \\ K_2 &> \bar{\Gamma}_2 + \frac{\varepsilon_3 L_0}{2m\delta_7} + \frac{\varepsilon_2\delta_3 K_2^2}{2} \\ K_3 &> \frac{\varepsilon_1}{2\delta_5 m} + \frac{\varepsilon_2 D_0}{2\delta_6 m} + \varepsilon_3\left(K_l L_0^2 + \frac{\bar{\Gamma}_3}{2\delta_8}\right) + \frac{\varepsilon_3\delta_9 K_3^2}{2} \end{aligned} \tag{47}$$

where $\bar{\Gamma}_1$ and $\bar{\Gamma}_2$ are defined in (26). Then, the trajectories of the closed-loop system resulting from (39) with control action (43) in which $\bar{u}$ is given in (21) and adaptive laws (22) and (44) are bounded, and $(z_1(t), z_2(t), z_3(t), \hat{\theta}(t), \hat{g}_l(t))$ converges to $(0,0,0,\theta,\bar{g}_l)$ globally, uniformly and exponentially.

Proof: By bering in mind the $\tilde{\theta}$ dynamics introduced in the proof of Proposition 3.1, and by letting $\tilde{g}_l := \hat{g}_l - g_l$, the closed-loop system in the error coordinates reads as

$$\begin{cases} \dot{z}_1 = z_2 \\ \dot{z}_2 = -K_1 z_1 - K_2 z_2 + \dfrac{z_3}{m} + \tilde{\theta}^{\mathrm{T}}\Theta - \\ \qquad\qquad - \dfrac{1}{m}\big[F_f(z_2 + x_2^\star) - F_f(x_2^\star)\big] \\ \dot{z}_3 = -\dfrac{z_2}{m} - K_3 z_3 + \tilde{g}_l G_l'(z_e,t) f_3'(z_1,t) \\ \dot{\tilde{\theta}} = -\left[\varepsilon_1 z_1 + z_2\right] K_\theta \Theta \\ \dot{\tilde{g}}_l = u_l \end{cases} \tag{48}$$

since $\dot{g}_l = 0$, and with u_l given by the right-hand side of (44). Consider now the Lyapunov function

$$V_4(z_1, z_2, z_3, \tilde{\theta}, \tilde{g}_l) := W_1(z_1, z_2, \tilde{\theta}) + \frac{1}{2}z_3^2 + \frac{1}{2K_l}\tilde{g}_l^2 \tag{49}$$

where K_l is a positive gain. From (36), we have that

$$\dot{V}_4(z_1, z_2, z_3, \tilde{\theta}, \tilde{g}_l) \leq -\Gamma_1 z_1^2 - \Gamma_2 z_2^2 - \varepsilon_2\Gamma_\theta\left\|\tilde{\theta}\right\|^2 - \\ - K_3 z_3^2 + \left(\varepsilon_1 z_1 + \varepsilon_2\tilde{\theta}^{\mathrm{T}}\Theta\right)\frac{z_3}{m} + z_3\Theta_l\tilde{g}_l + \tilde{g}_l\frac{u_l}{K_l}$$

where the definition of Θ_l given in (40) has been taken into account. By using the Young's inequality and since u_l is as in the right side of (44), we obtain that

$$\dot{V}_4(z_1, z_2, z_3, \tilde{\theta}, \tilde{g}_l) \leq -\left(\Gamma_1 - \frac{\varepsilon_1\delta_5}{2m}\right)z_1^2 - \Gamma_2 z_2^2 - \\ - \left(K_3 - \frac{\varepsilon_1}{2\delta_5 m} - \frac{\varepsilon_2 D_0}{2\delta_6 m}\right)z_3^2 - \\ - \varepsilon_2\left(\Gamma_\theta - \frac{\delta_6 D_0}{2m}\right)\left\|\tilde{\theta}\right\|^2$$

where δ_5 and δ_6 are arbitrary positive numbers. By the indicated choices of K_1, K_2, and K_3 in (47) with $\varepsilon_3 = 0$, we have that $\dot{V}_4(z_1, z_2, z_3, \tilde{\theta}, \tilde{g}_l) \leq 0$. This fact implies that the trajectories of the closed-loop system (48) are bounded. To prove that $(z_1, z_2, z_3, \tilde{\theta}, \tilde{g}_l)$ goes to zero globally and exponentially, we follow the same approach used in the proof of Proposition 3.1, i.e. we consider the functions

$$V_5(z_3, \tilde{g}_l) := z_3 \tilde{g}_l \Theta_l, \tag{50}$$

$$V_6(\tilde{g}_l) := \frac{1}{T_l} \tilde{g}_l^2 \int_{t-T_l}^{t} \int_{\bar{\tau}}^{t} \Theta_l^2(\tau) \, \mathrm{d}\tau \, \mathrm{d}\bar{\tau}. \tag{51}$$

The variation of (50) along the trajectories of (48) is equal to

$$\dot{V}_5(z_3, \tilde{g}_l) = z_3 \tilde{g}_l \dot{\Theta}_l - K_l \Theta_l^2 z_3^2 + \\ + \tilde{g}_l \Theta_l \left(-\frac{z_2}{m} - K_3 z_3 + \tilde{g}_l \Theta_l \right)$$

while, for (51), we can write that

$$\begin{aligned} \dot{V}_6(\tilde{g}_l) = & -\frac{2}{T_l} K_l \Theta_l z_3 \tilde{g}_l \int_{t-T_l}^{t} \int_{\bar{\tau}}^{t} \Theta_l^2(\tau) \, \mathrm{d}\tau \, \mathrm{d}\bar{\tau} + \\ & + (\tilde{g}_l \Theta_l)^2 - \frac{1}{T} \tilde{g}_l^2 \int_{t-T_l}^{t} \Theta_l^2(\tau) \, \mathrm{d}\tau \\ & \leq T_l K_l L_0^3 |\tilde{g}_l| |z_3| + (\tilde{g}_l \Theta_l)^2 - \frac{\mu_l}{T_l} \tilde{g}_l^2 \end{aligned}$$

where the first condition in (41) and the persistency of excitation hypothesis (42) have been taken into account. Now, with (49), (50) and (51) in mind, let us introduce the function

$$W_2(z_1, z_2, z_3, \tilde{\theta}, \tilde{g}_l) := V_4(z_1, z_2, z_3, \tilde{\theta}, \tilde{g}_l) - \\ - \varepsilon_3 V_5(z_3, \tilde{g}_l) + \varepsilon_3 V_6(\tilde{g}_l)$$

for which it is possible to prove that, if $\varepsilon_3 > 0$ is sufficiently small, there exist $\bar{\alpha}_1, \bar{\alpha}_2 > 0$ such that

$$\bar{\alpha}_1 \left\| \begin{pmatrix} z_1 & z_2 & z_3 & \tilde{\theta} & \tilde{g}_l \end{pmatrix}^{\mathrm{T}} \right\|^2 \leq W_2(z_1, z_2, z_3, \tilde{\theta}, \tilde{g}_l) \leq \\ \leq \bar{\alpha}_2 \left\| \begin{pmatrix} z_1 & z_2 & z_3 & \tilde{\theta} & \tilde{g}_l \end{pmatrix}^{\mathrm{T}} \right\|^2. \tag{52}$$

Under the conditions of Assumptions 3.2 and 3.3, along the trajectories of (48), we have that

$$\begin{aligned} W_2(z_1, z_2, z_3, \tilde{\theta}, \tilde{g}_l) \leq & -\left(\Gamma_1 - \frac{\varepsilon_1 \delta_5}{2m} \right) z_1^2 - \Gamma_2 z_2^2 - \\ & - \left(K_3 - \frac{\varepsilon_1}{2\delta_5 m} - \frac{\varepsilon_2 D_0}{2\delta_6 m} - \varepsilon_3 K_l \Theta_l^2 \right) z_3^2 - \\ & - \varepsilon_2 \left(\Gamma_\theta - \frac{\delta_6 D_0}{2m} \right) \left\| \tilde{\theta} \right\|^2 - \frac{\varepsilon_3 \mu_l}{T_l} \tilde{g}_l^2 + \\ & + \frac{\varepsilon_3}{m} |\Theta_l| |z_2| |\tilde{g}_l| + \\ & + \varepsilon_3 \left(T_l K_l L_0^3 + |\dot{\Theta}_l| + K_3 \right) |z_3| |\tilde{g}_l|. \end{aligned}$$

By using the Young's inequality, we obtain that

$$\dot{W}_2(z_1, z_2, z_3, \tilde{\theta}, \tilde{g}_l) \leq -\Gamma_1' z_1^2 - \Gamma_2' z_2^2 - \Gamma_3 z_3^2 - \\ - \varepsilon_2 \Gamma_\theta' \left\| \tilde{\theta} \right\|^2 - \varepsilon_3 \Gamma_l \tilde{g}_l^2 \tag{53}$$

where

$$\begin{aligned} \Gamma_1' &:= \Gamma_1 - \frac{\varepsilon_1 \delta_5}{2m} \\ \Gamma_2' &:= \Gamma_2 - \frac{\varepsilon_3 L_0}{2m\delta_7} \\ \Gamma_3 &:= K_3 - \frac{\varepsilon_1}{2\delta_5 m} - \frac{\varepsilon_2 D_0}{2\delta_6 m} - \\ & \quad - \varepsilon_3 \left(K_l L_0^2 + \frac{\bar{\Gamma}_3}{2\delta_8} + \frac{\delta_9 K_3^2}{2} \right) \\ \Gamma_\theta' &:= \Gamma_\theta - \frac{\delta_6 D_0}{2m} \\ \Gamma_l &:= \frac{\mu_l}{T_l} - \frac{L_0 \delta_7}{2m} - \frac{\bar{\Gamma}_3 \delta_8}{2} - \frac{1}{2\delta_9} \end{aligned} \tag{54}$$

with Γ_1, Γ_2, and Γ_θ defined in (37), and $\bar{\Gamma}_3$ in (46). If K_1, K_2 and K_3 are selected so that (47) holds, and if the constants ε_i, $i = 1, \ldots, 3$ and δ_j, $j = 1, \ldots, 8$, are chosen so that the hypotheses of the proposition are met, which implies that (45) holds true, then the gains defined in (54) are positive. Consequently, from (53), if $\Gamma' := \min\{\Gamma_1', \Gamma_2', \Gamma_3, \varepsilon_2 \Gamma_\theta', \varepsilon_3 \Gamma_l\}$, we obtain that

$$\dot{W}_2(z_1, z_2, z_3, \tilde{\theta}, \tilde{g}_l) \leq -\Gamma' \left\| \begin{pmatrix} z_1 & z_2 & z_3 & \tilde{\theta} & \tilde{g}_l \end{pmatrix}^{\mathrm{T}} \right\|^2 \tag{55}$$

with $\Gamma' > 0$. To prove that $(z_1(t), z_2(t), z_3(t), \tilde{\theta}_\theta(t), \tilde{g}_l(t))$ globally converges to zero exponentially and uniformly in the initial conditions, we consider relations (52) and (55), and then we proceed in the same way as in the proof of Proposition 3.1. ■

In the previous proposition, it is proved that when $q_{leak}(t)$ is given by (12) with $g_l(t) = \bar{g}_l \geq 0$, the origin of (48) is a global and exponentially stable equilibrium. However, in a real-world scenario, the "leakage gain" $g_l(t)$ is not constant, but it increases in time. This variation is largely slower than the dynamics associated with the single production cycle, so the overall system presents a multi-time-scale behaviour. To study what kind of performance degradation the leakage dynamic causes in the controlled system, we rely on the singular perturbations theory, see e.g. [14, Chapter 9]. With an eye on (48) in which $\tilde{\theta} := \hat{\theta} - \theta$ and $\tilde{g}_l := \hat{g}_l - g_l$, and with the dynamic of ξ_θ and ξ_l specified by (22) and (44), the overall dynamic is described by:

$$\begin{cases} \dot{z}_1 = z_2 \\ \dot{z}_2 = -K_1 z_1 - K_2 z_2 + \dfrac{z_3}{m} + \left(\hat{\theta} - \theta \right)^{\mathrm{T}} \Theta - \\ \qquad\qquad - \dfrac{1}{m} \left[F_f(z_2 + x_2^\star) - F_f(x_2^\star) \right] \\ \dot{z}_3 = -\dfrac{z_2}{m} - K_3 z_3 + (\hat{g}_l - g_l) G_l'(z_e, t) f_3'(z_1, t) \\ \dot{\hat{\theta}} = -\left[\varepsilon_1 z_1 + z_2 \right] K_\theta \Theta \\ \dot{\hat{g}}_l = -K_l G_l'(z_e, t) f_3'(z_1, t) z_3 \\ \dot{g}_l = \varepsilon_l^2. \end{cases} \tag{56}$$

The motivation behind the choice of the "leakage gain" dynamics reported in the last relation of (56) is that ε_l^{-1} is associated to the time constant of the controlled system performing a certain number of production cycles. As a

consequence, the rate of variations of g_l is several orders of magnitude lower than the time derivatives of the signals that characterise the plant dynamics.

Following [14, Chapter 9], denote by X and Z the states variables of the slow and of the fast dynamics, with X that plays the role of g_l, and Z of $(z_1, z_2, z_3, \hat{\theta}, \hat{g}_l)$. If $\tau = \varepsilon_l t$ represents the scaled time variable, (56) can be described by the standard singular perturbation model

$$\begin{aligned} \dot{X}(\tau) &= \mathcal{F}(\varepsilon_l) \\ \varepsilon_l \dot{Z}(\tau) &= \mathcal{G}(\tau, X(\tau), Z(\tau), \varepsilon_l) \end{aligned} \tag{57}$$

with initial conditions $X(0)$ and $Z(0)$ that depend smoothly on $\varepsilon_l > 0$. In (57), it is immediate that, from (56), $\mathcal{F}(\varepsilon_l) = \varepsilon_l$, while the expression of $\mathcal{G}(t, X, Z, \varepsilon_l)$ follows after some simple passages. When $\varepsilon_l = 0$, the second equation in (57) degenerates into $0 = \mathcal{G}(t, X, Z, 0)$ and yields the "quasi-steady-state" trajectories $\bar{Z} = \mathcal{H}(t, \bar{X}) = (0, 0, 0, \theta, \bar{g}_l)$, being $\bar{X} = \bar{g}_l$ the solution of the first equation in (57) when $\varepsilon_l = 0$. Note that the solutions of $0 = \mathcal{G}(t, X, Z, 0)$ are real and isolated. The next proposition characterises the evolution of $Z(\tau)$, solution of (57) when $\varepsilon_l > 0$ and small, against the quasi-steady-state trajectory $\bar{Z}$. The result is that an upper bound for $\left\| Z(\tau) - \bar{Z} \right\|$ is determined.

Proposition 3.3: Assume that the conditions of Proposition 3.2 holds true, except for the fact that, as reported in (56), $q_{leak}(t)$ defined in (12) is such that $\dot{g}_l(t) = \varepsilon_l^2$, with $g_l(0) = \bar{g}_l$ and $\varepsilon_l > 0$. For the closed-loop system (56), for any finite $t_0, t_1 > 0$ such that $t_0 < t_1$, there exist positive constants η and $\varepsilon_l^\star$ such that for all initial conditions

$$\left\| \begin{pmatrix} z_1(0) & z_2(0) & z_3(0) & \hat{\theta}(0) - \theta & \hat{g}_l(0) - \bar{g}_l \end{pmatrix}^{\mathrm{T}} \right\| < \eta,$$

and for all positive $\varepsilon_l \leq \varepsilon_l^\star$, we have that

$$\left\| \begin{pmatrix} z_1(t) & z_2(t) & z_3(t) & \hat{\theta}(t) - \theta & \hat{g}_l(t) - \bar{g}_l \end{pmatrix}^{\mathrm{T}} \right\| \leq O(\varepsilon_l) \tag{58}$$

uniformly for $t \in [t_0, t_1]$.

Proof: This result is a consequence of [14, Theorem 9.1]. In fact, it is easy to check that the singular perturbation model (57) that corresponds to (56) is such that the trajectories are bounded on some finite interval $[0, \tau_1]$, with $\tau_1 = \varepsilon_l t_1$, and that the functions $\mathcal{F}$, $\mathcal{G}$ and $\mathcal{H}$ are of class C^1. The exponential stability of the origin of (48) implies that also the origin of the so-called boundary layer model is exponentially stable. Then, the hypotheses of [14, Theorem 9.1] are met and the result immediately follows. ■

On a finite interval, the effect of the slow dynamics associated to the leakage is thus compensated by the control law (43). In a real-world scenario, since $\varepsilon_l \simeq 0$, relation (58) assures that the performance degradation is neglectable. It is worth noticing that the validity on a finite interval *only* is due to the fact the the leakage dynamic is assumed to be simply stable. If some convergence properties are assumed, the result can be extended on an infinite time interval. For example, this is possible if the slow dynamics is given by $\dot{X}(\tau) = \mathcal{F}(\tau, X(\tau), Z(\tau), \varepsilon_l)$ and the origin of the reduced model $\dot{X}(\tau) = \mathcal{F}(\tau, X(\tau), \mathcal{H}(\tau, X(\tau)), 0)$ is exponentially stable, [14, Theorem 9.4]. A rigorous analysis of this problem is however beyond the scopes of this paper.

m	150 kg	A_1	7696.90 mm^2
C_v	7000 Nm/s	A_2	3926.99 mm^2
V_{01}	1.0 mm^3	V_{02}	1.0 mm^3
β_e	1.49 GPa		

TABLE I: Nominal parameters of the plant model (7). As discussed in Section II-B, the areas A_1 and A_2 take into account the fact that the axis consists of two equal pistons in parallel and for which the diameters of the chambers 1 and 2 are 70 mm and 50 mm, respectively.

IV. Simulations

In this section, different simulation results are reported. In Section IV-A, the Simscape model of the plant is validated against experimental data, thus proving that it is a reliable virtual benchmark to test the control algorithms. In Section IV-B, the tracking performances in a single working cycle when no leakage is present are illustrated. In Section IV-C, the behaviour of the controlled plant in case of multiple working cycles characterised by an increasing leakage is presented to show the effectiveness of the leakage estimator loop.

A. Simscape model validation

The parameters of the model for control design presented in Section II-B are reported in Table I, with C_{01} and C_{02} computed by (6). In the same model, the presence of pipes in the hydraulic axis has been completely neglected. Such pipes are denoted by DN$_i$, $i = 1, \ldots, 4$, in Fig. 1. The idea is that the associated "second-order" effects can be compensated by the adaptive loop proposed in Proposition 3.1. However, in the Simscape model, such pipes are taken into account and their dynamics is described using a built-in element, whose viscoelastic parameters are taken from data sheets or obtained via experiments.

The 4-ways valve is characterised by a nonlinear and asymmetric characteristic, reported in Fig. 2. Following [15], a custom Simscape component has been developed. It consists of 4 different orifices and an algebraic map that relates the opening of the spools with the command set point of the valve. To determine such map, simulations are performed by varying the valve command from 0 mm to its maximum. The corresponding characteristic curve is matched with the one in the data-sheet, and the error drives a least square algorithm that is designed to find the "optimal" map between the opening of the spools and the command set point. In Fig. 4, the comparison between the characteristics of the real valve and the one of the Simscape model are reported for the PB way. Similar results have been obtained for the PA, AT, and BT ones. Moreover, in Fig. 5, the achieved results are compared to experimental data. The system is in open-loop and driven by the spool command reported in the bottom graph. When 10 V are applied, the maximum value of the spool opening, i.e. 3 mm, is reached. The velocity of the piston obtained by the Simscape model is in good accordance with the measurements on the real system.

One of the main requirements is to estimate and compensate for the leakage in the hydraulic circuit. The emphasis here is

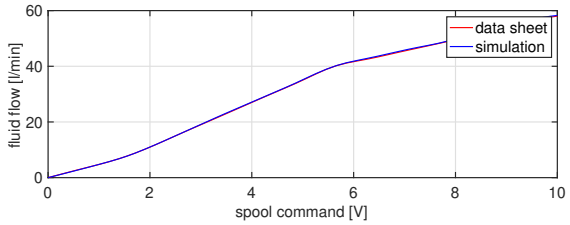

Fig. 4: Comparison between the static characteristics of the real valve and of the associated Simscape model at nominal pressure drop for the PB way / orifice.

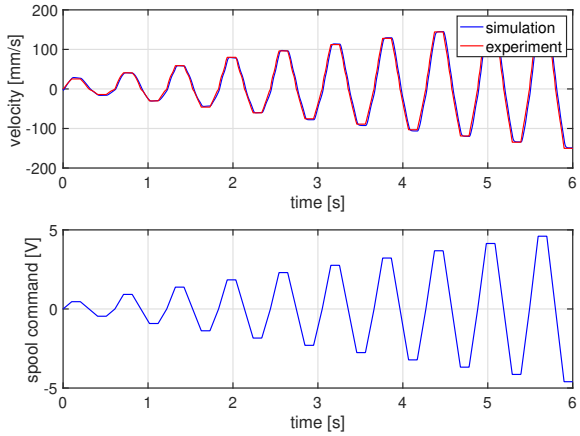

Fig. 5: Behaviour of the Simscape model for a specific spool command, and comparison with experimental data.

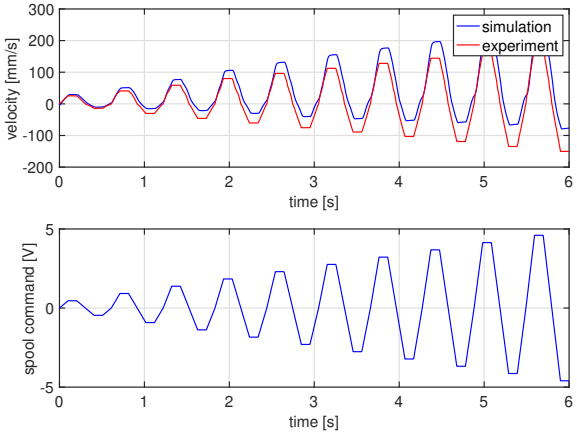

Fig. 6: Behaviour when internal leakage increases: comparison between the nominal behaviour of the cylinder (taken from experiments) and of the Simscape model.

K_1	5e6	K_2	1e4
K_3	150	ε_1	80
K_θ	1e6	K_l	1e-17

TABLE II: Parameters of the regulator of Proposition 3.2 used in the simulations of Section IV. With some abuse in notation, here K_θ denotes a gain that multiplies the identity matrix of order $N_f + N_d$ to get the corresponding K_θ matrix in the adaptive law (22).

on the leakage in the piston only, modelled using an orifice connected between the two chambers, see (2) and (12). The tuning of the parameters is based on collected data that lead to an upper limit of the total leakage flow of 15 l/min in nominal conditions. Since such phenomenon is unpredictable and quite difficult to measure and quantify, it is not possible to compare the response obtained in simulation against real data, so just the effects on the system performances of an increasing leakage are reported. The results are in Fig. 6, where the spool opening associated with the orifice has been increased after each cycle. The response is compared to the static characteristic of the real machine. As expected, performances get worse as long as leakage intensifies as if an increasing offset on the command law of the valve is introduced. This justifies why in the experiments reported in Section V-B, leakage in the piston is artificially introduced by summing a constant and unknown offset to the spool command.

B. Single cycle with no leakage

The control algorithm developed in Section III is validated on the Simscape mode. It is supposed that no leakage is present. This means that, in Proposition 3.2, $K_l = 0$, i.e. only the adaptive loop that compensate for the external force and disturbances acting on the piston is active. The plant parameters are summarised in Table I, while the gains in the control law are reported in Table II. These parameters have been determined by exploiting the inner-outer loop structure of the controller. The gains of the outer loop are selected to get the desired response (or bandwidth) for the mechanical subsystem. Then, the inner-loop is tuned to be "sufficiently faster." In the model of the friction effects (9), we have assumed that $N_f = 2$ with $\Phi_1(x_2^\star) = 1$ and $\Phi_2(x_2^\star) = x_2^\star$. The first function is meant to compensate for dry friction, while the second one is related to viscous friction and "corrects" the feedforward term $C_v x_2^\star$ that appears in (21). Note that, to deal with dry friction in a rigorous manner, it would have been preferable to have $\Phi_1(x_2^\star) = \operatorname{sign} x_2^\star$. The reference trajectory (see Fig. 7) is characterised by only one inversion of the velocity during the cycle, so the adaptive loop is required to change the sign of the estimate of ϕ_1 only once, and this transient is not deteriorating the tracking error beyond the desired threshold. In addition, the actual choice for Φ_1 adds a (nonlinear) integral action that is beneficial for the overall performances.

In the first simulation, a single working cycle with no external force and no leakage is performed. The reference trajectory is reported in Fig. 7. The adaptive loop on the friction force and on the external disturbances is active, and the performances in terms of position tracking error are illustrated in Fig. 8a. In (10), we have assumed that $F_{ext}(x_1) = 0$, while in (11) that $N_d = 1$ and $\Gamma_1(t) = 1$. This choice is motivated by the fact that in this case the disturbance acting on the mechanical subsystem is mainly due to the pressure loss in the pipes, and so it can be easily compensated by an integral action. Note that the steady-state error is zero, and

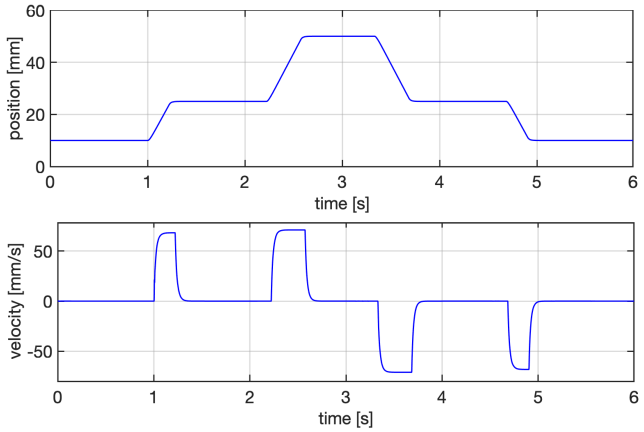

Fig. 7: Position (top) and velocity (bottom) profiles of the trajectory used in the working cycle.

that the maximum tracking error is equal to 0.03 mm. As far as the velocity tracking error is concerned, the achieved performances are illustrated in Fig. 8b. The velocity profile is tracked accurately, and the maximum tracking error is equal to 5.40 mm/s. The corresponding control input, i.e. the spool command, is reported in Fig. 9c. Finally, in Fig. 8d, the contribution of the adaptive loop is shown. Even if no external force is acting on the piston, the adaptive loop has to compensate for several non idealities in the plant, that are not taken into account in the control design. Among them, pressure drops caused by by laminar / turbulent motion, and elastic effects due to fluid compressibility.

In a second simulation, the same reference trajectory of Fig. 7 is employed, but with the addition of an external force whose profile is reported in Fig. 9d. Such external force is caused by the compression of the powder in the mould during the production. It is worth pointing out that such external force is *not* the pressing force, but it is strongly related to it. In fact, the pressing force acts on the main hydraulic axes in the press, while the auxiliary ones, such as the Y_2 presented here, are at mechanical end-stop during the pressing phase. For such auxiliary axes, it is fundamental that the steady-state error is as much close as possible to zero. A steady-state error larger than 0.01 mm could cause problems in the next pressing phase. To deal with such an external disturbance, in (10) we still assume that $F_{ext}(x_1) = 0$, while in (11) that $N_d = 2$ with $\Gamma_1(t) = 1$ as before, and $\Gamma_2(t)$ equal to a "scaled" version of the curve in Fig. 9d which describes the force acting on the piston. It is clear that this is the worst case scenario and that better performances could have been obtained by properly defining the feedforward term $F_{ext}(x_1)$. As illustrated in Fig. 9a, the position tracking performances are quite similar to the case in which such external force is not present. The maximum tracking error is equal to 0.38 mm and reached in the transient phase. As far as the velocity tracking error is concerned, the result is in Fig. 9b, and the same considerations drawn for the position tracking error are still valid; the maximum value is equal to 5.40 mm/s. To conclude, the control input and contribution of the adaptive loop are presented in Figures 9c and 9d, respectively. Note that the adaptive loop is capable to match such external force and to compensate for it perfectly.

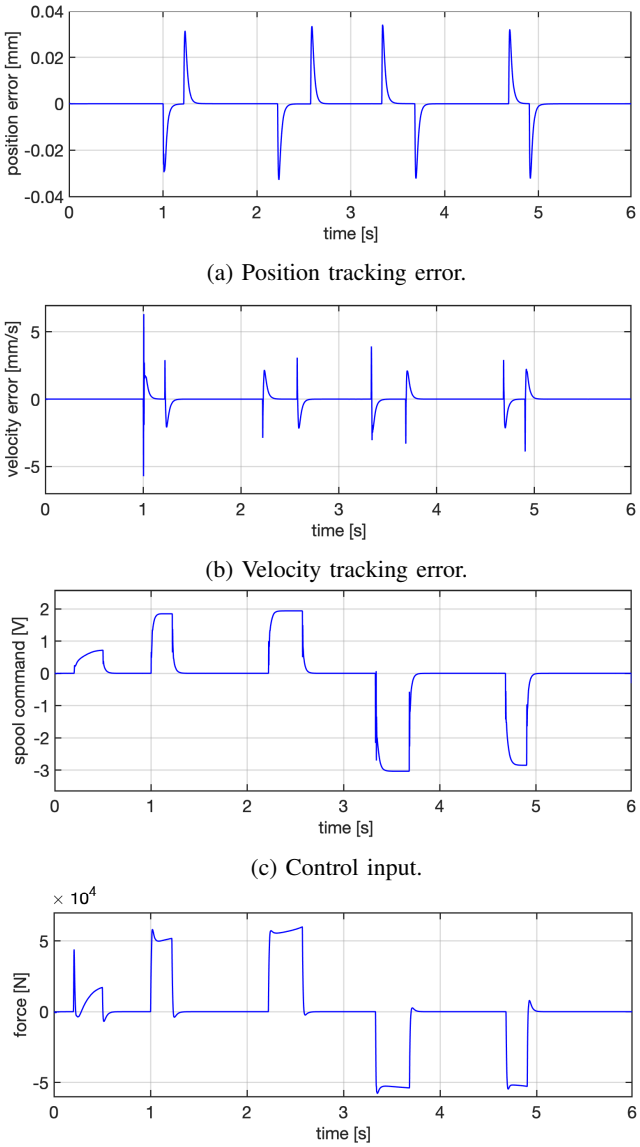

(a) Position tracking error.

(b) Velocity tracking error.

(c) Control input.

(d) Contribution of the adaptive loop on the force.

Fig. 8: Working cycle with no external force and no leakage: behaviour of the controller of Proposition 3.2 with $K_l = 0$.

C. Repeated cycles with increasing leakage

The scope of the simulations reported in this section is to show the performances that can be achieved with the complete control scheme of Proposition 3.2 not only in terms of the external force / disturbances compensation but also in case of leakage in the piston. The press undergoes several working cycles, i.e. different repetitions of the trajectory employed in Section IV-B, see the top graph in Fig. 7. At the same time, leakage flow is simulated using (2) with a nominal discharge coefficient $C_{0l} = 0.1323\,\mathrm{l\,bar^{0.5}/(min\,mm)}$, and an opening $x_l(t)$ that varies as reported in red in Fig. 10c. The value of C_{0l} has been computed to have a nominal flow of 1.68 l/min at a nominal pressure drop of 10 bar when $x_l = 3\,\mathrm{mm}$. Plant

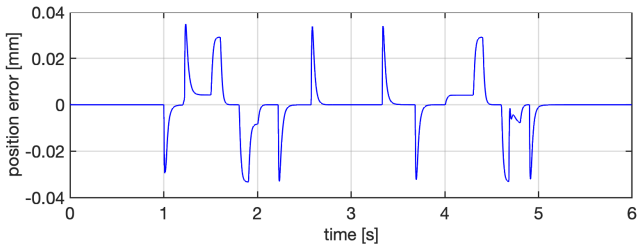

(a) Position tracking error.

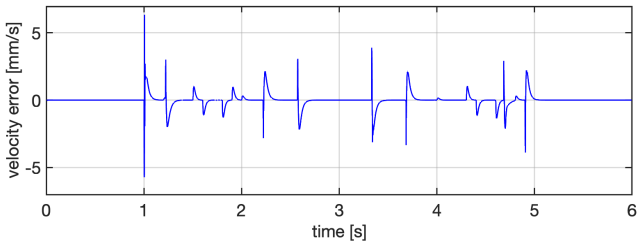

(b) Velocity tracking error.

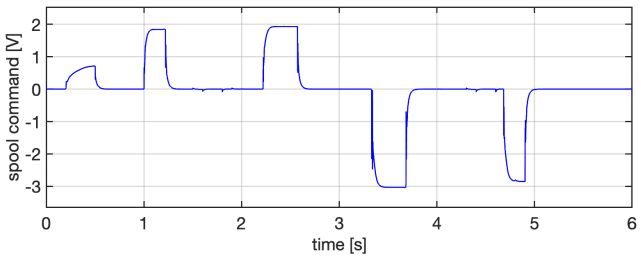

(c) Control input.

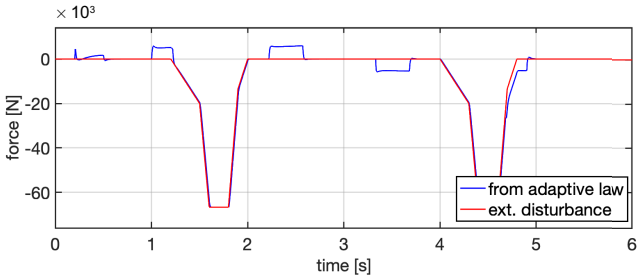

(d) External force and contribution of the adaptive loop on the force.

Fig. 9: Working cycle with external force and no leakage: behaviour of the controller of Proposition 3.2 with $K_l = 0$.

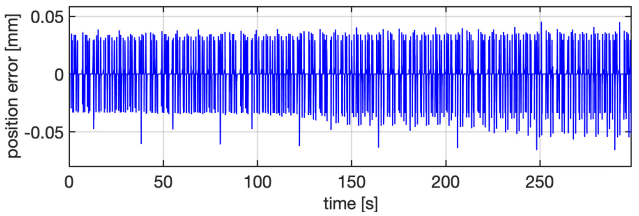

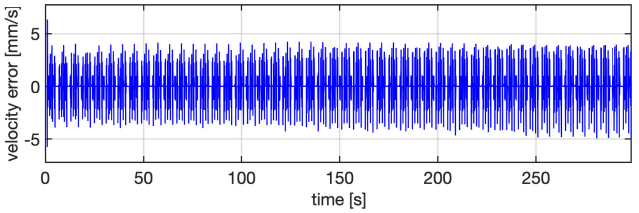

(a) Position and velocity errors.

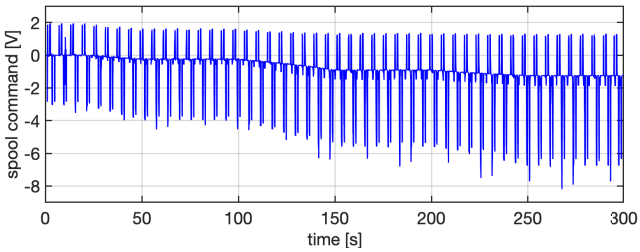

(b) Control input.

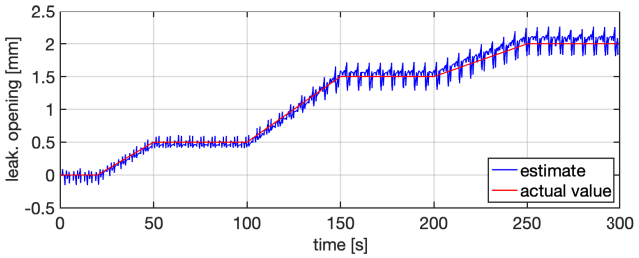

(c) Leakage opening and its estimate.

Fig. 10: Multiple working cycles with external force and leakage: behaviour of the controller of Proposition 3.2.

parameters and control gains are summarised in Tables I and II, respectively.

Even in this case, the controller assures good performances, since both the force and leakage adaptive loops can compensate for such external disturbances. As reported in Fig. 10a, position and velocity tracking errors remain of the same magnitude as in case no leakage is present. More precisely, the maximum position tracking error is lower than 0.05 mm, while the maximum velocity tracking error than 5.00 mm/s. The evolution of the spool command is reported in Fig. 10b, while the estimate of the leakage opening is in Fig. 10c. Note that in a real-world scenario the leakage dynamics is largely slower than the one simulated here. Such levels of internal leakage are reached after hundred thousands of cycles and usually the system is stopped for maintenance when the intensity of the undesired flow is comparable to the one associated to an x_l of $1 \div 1.5$ mm in (2). The adaptive loop correctly estimates the leakage, and such information is successfully employed in the control loop to let the system having acceptable performances even in these extreme situations. The ripple that can be noted in the estimate is because the adaptive loop is influenced also by the force dynamics. What happens is that to follow the leakage opening profile of Fig. 10c, the gain of the associated adaptive loop is larger than necessary, i.e. than the one that would be employed in reality.

V. Experiments

In this section, two experiments are presented to show the behaviour of the real system. In Section V-A, the performances obtained in a single cycle with no leakage are reported and compared with the ones of the PID with feedforward action currently implemented. In Section V-B, the response recorded in several working cycles with increasing leakage is shown, and the effectiveness of the corresponding estimator is verified. Since the press and its control algorithm are still

K_1	3.5e6	K_2	2e3
K_3	80	ε_1	80
K_θ	1e6$\times I_{N_f+N_d}$	K_l	1e-17

TABLE III: Parameters of the regulator of Propositions 3.1 and 3.2 used in the experiments of Section V. In the same way as in Section IV, here K_θ denotes a gain that multiplies the identity matrix of order $N_f + N_d$ to get the corresponding K_θ matrix in the adaptive law (22).

in a prototype phase, in all the experiments no pressing has been carried out to preserve the mould, which is quite fragile (and expensive). So, the adaptive loop of Proposition 3.1 is employed to estimate friction forces and unmodelled external disturbances, but not the contact forces generated during the pressing phase. Consequently, as in Section IV-B, in (9), we have that $N_f = 2$, with $\Phi_1(x_2^\star) = 1$ and $\Phi_2(x_2^\star) = x_2^\star$. The same considerations related to the compensation of dry friction reported in Section IV-B remain valid also here. Furthermore, in (10) we have that $F_{ext}(x_1) = 0$, while in (11) that $N_d = 1$ and $\Gamma_1(t) = 1$. The controller parameters are selected as reported in Table III. Note that the inner loop gains have been reduced if compared to the ones employed in the simulations. If the reference trajectory of the experiments (see the top graph in Fig. 11), is compared with the one in the simulations (see the top graph in Fig. 7), it is possible to note a discontinuity in the velocity profile. This is because now the trajectory planner generates trapezoidal position profiles only. The experiments refer to the real working conditions of the system, but it reasonable to assume that with a smoother profile the overall performances would improve. The actual behaviour meets the requirements in term of either position and velocity tracking.

A. Single cycle with no leakage

This section aims to present the performances obtained by the control system of Proposition 3.2 with $K_l = 0$ in a single working with no leakage. The reference trajectory is depicted in the upper graph of Fig. 11, while in the lower one the tracking error obtained employing the PID with feedforward action and the adaptive controller of Proposition 3.2 are reported. The actual regulator in such ideal conditions assures a maximum tracking error of 0.33 mm. Such performances are mostly due to the feedforward action that has been experimentally defined and tuned on the specific axis and class of reference trajectories. The main issue is that the actual controller works very well until some small "perturbations" such as disturbances, wear-out of the components and oil temperature act on the system. The consequence is that the plant is characterised by a low level of repeatability and a relatively small robustness margin. As far as the tracking capabilities in position and velocity of the adaptive controller of Proposition 3.2 are concerned, the results are shown in Fig. 11 and in Fig. 12, respectively. Note that the tracking error slightly increases as compared to the PID regulator because the feedforward action is based on the simplified model of the plant (13). This can be easily seen by letting $\hat{g}_l = 0$ in (43). In these conditions, the maximum tracking error is equal to

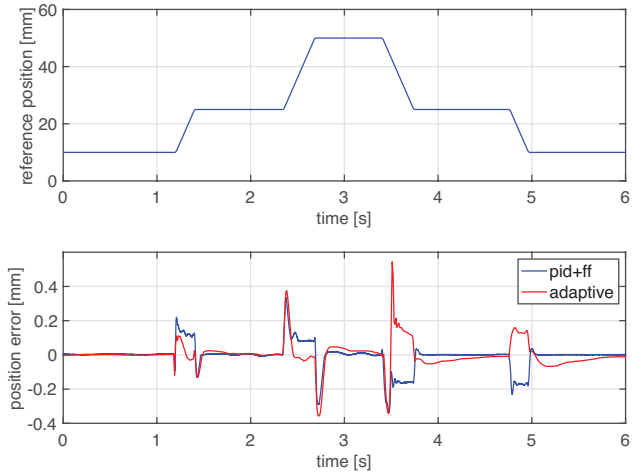

Fig. 11: Single working cycle with no leakage: position tracking obtained with the PID with feedforward action and with the adaptive controller.

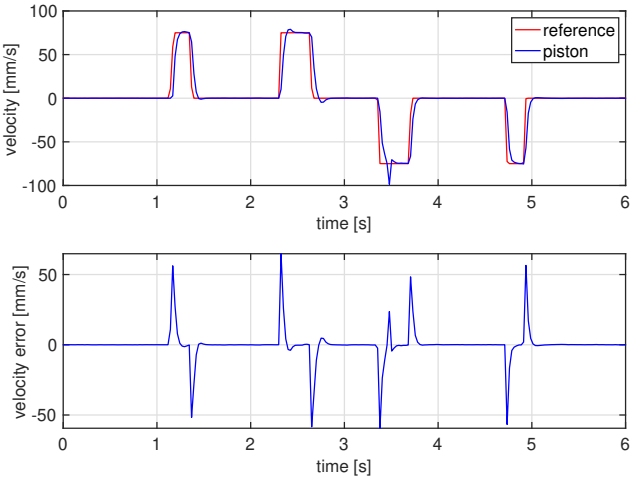

Fig. 12: Single working cycle with no leakage: velocity tracking achieved with the controller of Proposition 3.2.

0.58 mm, that is still acceptable; the steady state error is zero and the velocity tracking error is equal to 68.24 mm/s.

Even if in the experiment the pressing phase is not realised, the adaptive action on the external force is playing a crucial role in compensating, not only for the friction forces but also for the non-idealities of the pressure sensors and supply system. The evolution of the pressures P_1 and P_2 inside the cylinder, and of the pressure P_s of the supply system are reported in Fig. 13. As far as the pressures P_1 and P_2 are concerned, it is important to observe that the sensors are not placed inside the cylinder, but on the pipes that let the fluid in and out the corresponding chambers. Consequently, the adaptive loop is in charge of compensating the unmodelled pressure losses in such pipes, and also some other non-idealities related, for example to the fluid compressibility and the elasticity of the pipes themselves. Furthermore, the pressure P_s is non-constant and equal to 280 bar, as supposed,

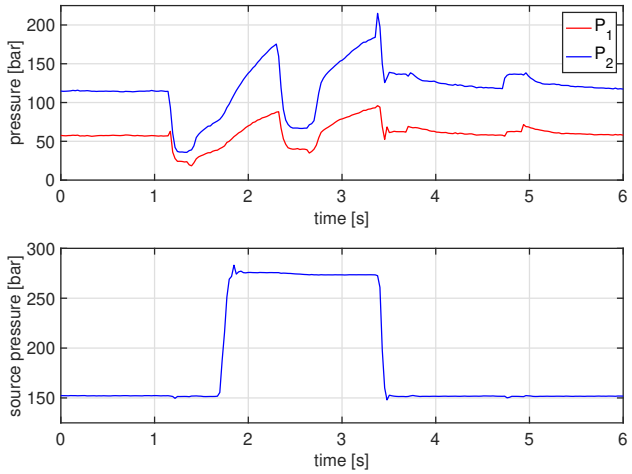

Fig. 13: Single working cycle with no leakage: pressures P_1 and P_2 inside the cylinder (top), and pressure P_s of the supply (bottom). The regulator is the one of Proposition 3.2.

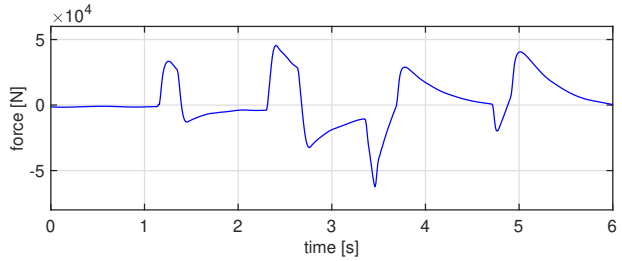

Fig. 14: Single working cycle with no leakage: contribution of the adaptive loop on the force introduced in Proposition 3.1.

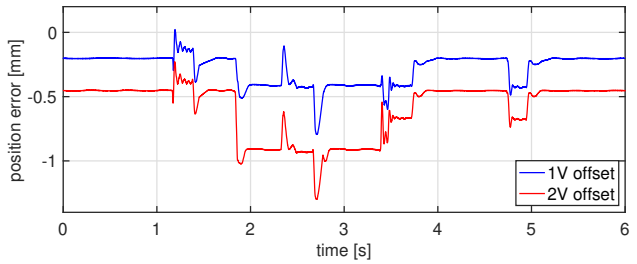

Fig. 15: Single working cycle with leakage: position tracking with the PID in case of different offsets.

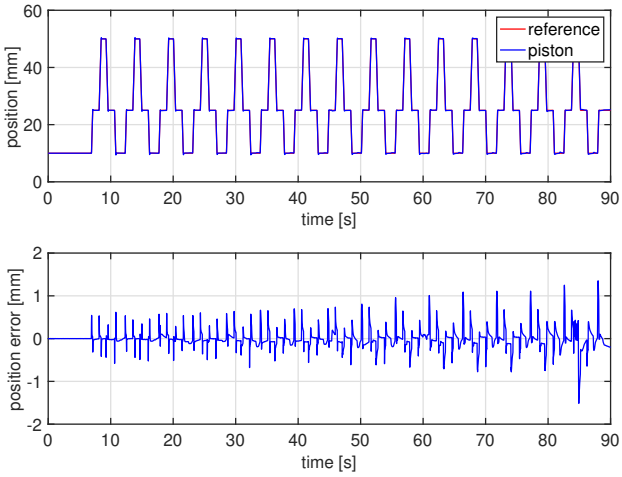

Fig. 16: Multiple working cycles with increasing leakage: position tracking achieved with the controller of Proposition 3.2.

but it varies during the working cycle, as reported in the bottom graph of Fig. 13. More precisely, the lower value is 141.04 bar, while the higher one is 283.10 bar. As a result, the adaptive loop generates the contribution depicted in Fig. 14 to compensate for these undesired effects.

B. Repeated cycles with increasing leakage

The performances that are achieved when leakage is present are discussed in this section. In the actual control system, it is assumed that the leakage flow is no longer neglectable once the tracking error goes beyond a threshold that has been determined empirically. Besides improving the tracking performances, the control scheme of Proposition 3.2 provides a more reliable and accurate "measure" of such an effect that can be employed for predictive maintenance.

With the considerations reported at the end of Section IV-A in mind, in these experiments, leakage is "virtually" generated by adding an unknown offset to the spool command. The reference trajectory is the same as in the top graph in Fig. 11. The behaviour of the plant with the actual regulator when the leakage is "simulated" by an offset on the spool command of 1 V and 2 V, respectively, is reported in Fig. 15. In the first case, the maximum error is equal to 0.79 mm, while in the second case to 1.29 mm. Even if not reported here, a single working cycle with leakage generated by an offset of 1,5 V has been analysed. The maximum tracking error that has been measured is equal to 1.04 mm. In real-world scenarios, when the tracking performances deteriorate as in the $1 \div 1.5$ V offset range, the press is stopped for maintenance.

To test the complete control scheme, the piston runs several working cycles with an increasing leakage. More precisely, as depicted in Fig. 18, bottom graph, the offset on the spool command varies from 0 V, i.e. no leakage, to 2.5 V with steps of 0.5 V. This is clearly an extreme situation that is not going to happen in practise. The performances obtained when tracking the desired position profile are reported in Fig. 16. The tracking error is slightly lower than in case of the PID with feedforward action. In particular, with an offset of 0.5 V, the maximum position tacking error is equal to 0.60 mm, with 1.0 V to 0.70 mm, with 1.5 V to 0.95 mm, and with 2.0 V to 1.08 mm. As far as the velocity tracking performances, the results are reported in Fig. 17. In particular, with an offset of 0.5 V, the maximum velocity tacking error is equal to 73.55 mm/s, with 1.0 V to 74.33 mm/s, with 1.5 V to 74.22 mm/s, and with 2.0 V to 65.43 mm/s. Finally, the behaviour of the force and leakage adaptive loops is reported in Fig. 18. Since the leakage varies with a dynamics that is comparable with the one associated with the reference trajectory, the force and leakage adaptive loops are coupled. In any case, the leakage adaptive loop provides a good estimate

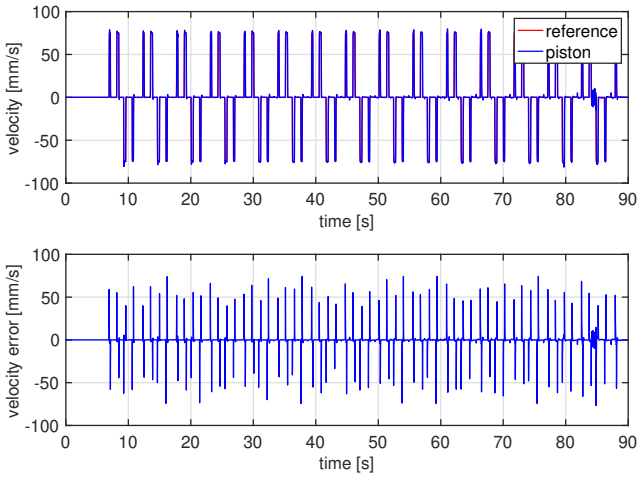

Fig. 17: Multiple working cycles with increasing leakage: velocity tracking achieved with the controller of Proposition 3.2.

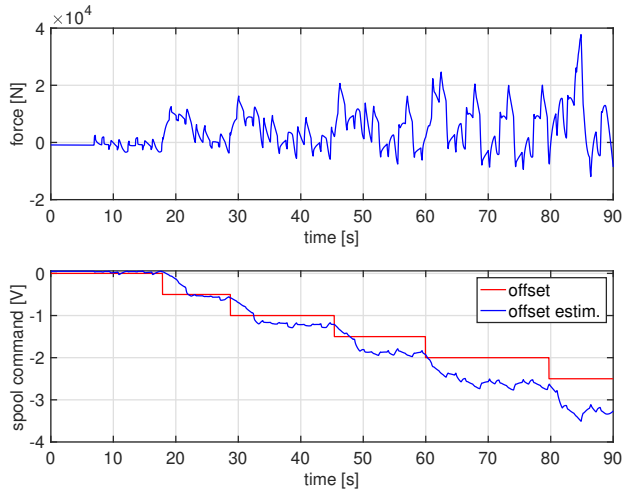

Fig. 18: Multiple working cycles with increasing leakage: contribution of the adaptive loop on the force (top) and on the leakage (bottom).

that is quite precise in particular in the range $1.0 \div 1.5$ V that corresponds to the situation in which the plant undergoes a maintenance procedure.

VI. Conclusions and Future Work

In this paper, the adaptive robust control of a hydraulic press has been presented. The design is based on classical backstepping arguments and the resulting control law is characterised by an inner / outer loop structure. In particular, the outer loop is responsible for the motion of the press having the hydraulic pressure acting on the piston as input, while the inner loop is in charge of generating such pressure by operating on a servo-valve. Besides, two adaptive laws are implemented. The first one is associated with the outer loop and is capable to compensate for the external forces generated during the pressing phase or due to some unmodelled effects, such as friction, fluid compressibility and non-idealities in the supply system. Instead, the second adaptive law is paired with the inner loop and is designed to compensate for the leakage flow in the servo valve, a major source of performance degradation in the system. In this respect, the leakage estimate is employed not only in the adaptive loop to compensate the leakage effect, but also for predictive maintenance, i.e. to let the user gather information about the internal state of the component. The validity and the performances that the control scheme provides are illustrated with the help of several simulations in which a detailed physical model of the plant has been employed. Then, experimental results are also presented, and a comparison with the actual control solution, a PID with feedforward action, is carried out. The structure and the overall complexity of the proposed controller is quite similar to the one of the actual PID with feedforward action, with the advantage that now the empiric determination of such a feedforward term is no longer necessary because a model-based design has been adopted. Moreover, the proposed adaptive controller is characterised by greater repeatability and reliability if compared to the PID. The latter assures a very limited stability margin: the result is those good performances are very difficult to be guaranteed in the long run. The consequence is that the press has to be stopped for software and hardware maintenance more frequently.

Future activities are focused on the design of an automatic tuning procedure to determine not only the "best" controller gains but also the functions to be employed in the adaptive loop on the disturbances acting on the mechanical subsystem. One of the main achievement of the proposed control solution is the possibility of having at disposal an estimate of the leakage in the piston. However, in a hydraulic press, leakage can also occur in the valve. The idea is then to estimate these two leakages flows to increase the robustness of the whole architecture. Besides, maintenance would be performed on the right component, thus reducing the length of the intervention and the period in which the machine is not operative.

References

[1] Y. Wang, F. Gao, and F. Doyle III, "Survey on iterative learning control, repetitive control, and run-to-run control," *Journal of Process Control*, vol. 19, no. 10, pp. 1589–1600, Dec. 2009.

[2] J. Xu, "A survey on iterative learning control for nonlinear systems," *International Journal of Control*, vol. 84, no. 7, pp. 1275–1294, 2011.

[3] B. Yao, "High performance adaptive robust control of nonlinear systems: A general framework and new schemes," in *Decision and Control (CDC 1997). Proceedings of the 36th IEEE Conference on*, San Diego, CA, USA, Dec. 1997, pp. 2489–2494.

[4] B. Yao and M. Tomikuza, "Adaptive robust control of SISO nonlinear systems in a semi-strict feedback form," *Automatica*, vol. 33, no. 5, pp. 893–900, May 1997.

[5] M. Krstic, I. Kanellakopoulos, and P. Kokotovic, *Nonlinear and adaptive control design*. New York, USA: Wiley-IEEE Press, 1995.

[6] R. Sepulchre, N. Jankovic, and P. Kokotovic, *Constructive Nonlinear Control*. New York, USA: Springer, 1997.

[7] F. Bu and B. Yao, "Nonlinear adaptive robust control of hydraulic actuators regulated by proportional directional control valves with deadband and nonlinear flow gains," in *American Control Conference (ACC 2000). Proceedings of the*, Chicago, IL, USA, Jun. 28-30 2000.

[8] B. Yao, F. Bu, J. Reedy, and G.-C. Chiu, "Adaptive robust motion control of single-rod hydraulic actuators: theory and experiments," *IEEE/ASME Transactions on Mechatronics*, vol. 5, no. 1, pp. 79–91, Mar. 2000.

[9] F. Bu and B. Yao, "Desired compensation adaptive robust control of single-rod electro-hydraulic actuator," in *American Control Conference (ACC 2001). Proceedings of the*, Arlington, VA, USA, Jun. 25-27 2001, pp. 3926–3931.

[10] B. Yao, F. Bu, and G.-C. Chiu, "Non-linear adaptive robust control of electro-hydraulic systems driven by double-rod actuators," *International Journal of Control*, vol. 74, no. 8, pp. 761–775, 2001.
[11] B. Yao, M. Al-Majed, and M. Tomikuza, "High performance robust motion control of machine tools: An adaptive robust control approach and comparative experiments," *IEEE/ASME Transactions on Mechatronics*, vol. 2, no. 2, pp. 63–76, 1997.
[12] B. Yao and M. Tomikuza, "Comparative experiments of robust and adaptive control with new robust adaptive controllers for robot manipulators," in *Decision and Control (CDC 1994). Proceedings of the 33th IEEE Conference on*, Orlando, FL, USA, 1994, pp. 1290–1295.
[13] ——, "Adaptive robust motion and force tracking control of robot manipulators in contact with compliant surfaces with unknown stiffness," *ASME Journal of Dynamic Systems, Measurement, and Control*, vol. 120, no. 2, pp. 232–240, 1998.
[14] H. Khalil, *Nonlinear Systems*, 2nd ed. Prentice Hall, 1996.
[15] C. Johny and K. Sivadas, "Simulation of pressure variation in hydraulic circuit with & without hydraulic accumulator in MATLAB-Simhydraulics," in *International Conference on Emerging Trends in Engineering & Management*, Jan. 2016, pp. 55–59.
[16] B. Eryilmaz and B. Wilson, "Modeling the internal leakage of hydraulic servovalves," in *International Mechanical Engineering Congress and Exposition, ASME*, vol. 69, 2000, pp. 337–343.
[17] J. Yao, Z. Jiao, and D. Ma, "A practical nonlinear adaptive control of hydraulic servomechanisms with periodic-like disturbances," *IEEE/ASME Transactions on Mechatronics*, vol. 20, no. 6, pp. 2752–2760, Dec. 2015.
[18] M. Polycarpou and P. Ioannou, "A robust adaptive nonlinear control design," in *Proceedings of the 1993 American Control Conference*, San Francisco, CA, USA, June 2-4 1993, pp. 1365–1369.
[19] J. Yao, Z. Jiao, D. Ma, and L. Yan, "High-accuracy tracking control of hydraulic rotary actuators with modeling uncertainties," *IEEE/ASME Transactions on Mechatronics*, vol. 19, no. 2, pp. 633–641, Apr. 2014.
[20] P. Ioannou and J. Sun, *Robust Adaptive Control*. Upper Saddle River, NJ, USA: Prentice Hall, 1985.
[21] F. Mazenc, M. De Querioz, and M. Malisoff, "Uniform global stability of a class of adaptively controlled nonlinear systems," *Automatic Control, IEEE Transactions on*, vol. 54, no. 5, pp. 1152–1158, May 2009.

Davide Barchi was born in Faenza, Italy in 1993. He got a master's degree in Automation Engineering at the University of Bologna in 2017. Since January 2018, he works in SACMI Innovation Lab as an R&D Software Engineer. He had experience in Robotics Application involving 3D Trajectory Planning and control. His current activity is mainly focused on research and development of simulation systems, design of automatic control systems and digital twins as well as virtual commissioning applications.

Alessandro Macchelli (M'06–SM'17) graduated in 2000 and took the Ph.D. degree in 2003 at the University of Bologna. In 2003 and 2004, he got Post-Doc positions at the University of Twente, and at the University of Bologna, respectively. In April 2005, he joined the Department of Electronics, Computer Science and Systems, DEIS (now Department of Electrical, Electronic and Information Engineering, DEI) as Assistant Professor. Now, he is an Associate Professor at the same department. He held visiting positions at various academic / research international institutions. His research activity is mainly focused on port-Hamiltonian systems, with particular emphasis on modelling, simulation and control of distributed parameter systems, and applications of the port-Hamiltonian framework to robotics and mechatronics. He is currently author of more than 80 journal and conference papers on these topics. He serves as Associate Editor for the *IEEE Transactions on Automatic Control* and for the *IEEE Transactions on Control Systems Technology.*

Gildo Bosi has begun his professional activity in the SACMI technical office in 1986 as automation systems designer. Since 2001, he is chief of the R&D automation department and coordinator of the SACMI Innovation Lab activities. He is member of the board of directors of the Mister Laboratory of the "Alta Tecnologia" network since 2005.

Lorenzo Marconi graduated in 1995 in Electrical Engineering from the University of Bologna. Since 1995 he has been with the Department of Electronics, Computer Science and Systems at University of Bologna, where he obtained his Ph.D. degree in 1998. From 1999 he has been an assistant professor in the same department where he is now a full professor. He has held visiting positions at various academic/research international institutions. He is a co-author of more than 250 technical publications on the subject of linear and nonlinear feedback designs published on international journals, books and conference proceedings. In 2005, he received the "Outstanding Application Paper Award" from IFAC for a coauthored paper published on Automatica. He is also the co-recipient of the 2014 IEEE Control Systems Magazine Outstanding Paper Award for the best paper published in the magazine in the period 2012-2013 and of the 2018 O. Hugo Schuck Best Paper Award. He is Fellow of IEEE for contributions to feedback design of nonlinear systems and unmanned aerial vehicles. His current research interests include nonlinear control, output regulation, control of autonomous vehicles, fault detection and isolation, and fault tolerant control.

Davide Foschi was born in Imola, Italy in 1973. He is currently the Technical Manager of the Advanced Technology Business Unit in SACMI IMOLA. He received a master's degree in Automation Engineering at the University of Bologna in 1998. He worked since 2007 on several projects regarding multi-axes hydraulic presses, focusing on closed-loop motion control.

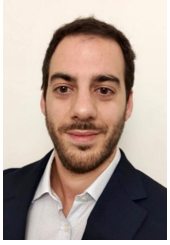

Mirco Mezzetti was born in Imola, Italy in 1989. He is currently the head of Automation Design Department of the Advanced Technology Business Unit in SACMI IMOLA. He received a master's degree in Automation Engineering at the University of Bologna in 2014. Since then, he worked on several projects regarding multi-axes hydraulic presses control, focusing on closed-loop motion system implementation and test.